



**JOURNAL OF INNOVATIVE<sup>®</sup>  
TRANSPORTATION**

**YEAR 2022**  
**VOLUME 3**  
**ISSUE 1**



## **EDITORS-IN-CHIEF**

**Professor Serdal Terzi, PhD**

 0000-0002-4776-824X

Suleyman Demirel University  
Department of Civil Engineering  
Isparta, Turkey

**Professor Mehmet Saltan, PhD**

 0000-0001-6221-4918

Suleyman Demirel University  
Department of Civil Engineering  
Isparta, Turkey

## **VICE EDITOR-IN-CHIEF**

**Associate Professor Şebnem Karahançer, PhD**

 0000-0001-7734-2365

Isparta University of Applied Sciences  
Department of Civil Engineering  
Isparta, Turkey

## **EDITORS**

**Professor Andreas Loizos, PhD**

National Technical University of Athens  
Athens, Greece

**Professor Erol Tutumluer, PhD**

University of Illinois Urbana-Champaign  
Urbana, IL, USA

**Professor Luis Picado-Santos, PhD**

University of Lisbon  
Lisbon, Portugal

**Professor Ali Khodaii, PhD**

Amirkabir University of Technology  
Tehran, Iran

**Professor Othman Hamzah, PhD**

University Sains Malaysia  
George Town, Malaysia

**Associate Professor Burak F. Tanyu, PhD**

George Mason University  
Fairfax, VA, USA



## Investigation of the correlation between California bearing ratio and shear strength of pavement subgrade material with different water contents

Süleyman Gökova<sup>a,\*</sup>

<sup>a</sup>Department of Land Registry and Cadastre, Gölhisar School of Applied Sciences, Mehmet Akif Ersoy University, Burdur, Turkey

### Highlights

- CBR and shear strength of subgrade soil were found experimentally
- The effect of the water content on CBR and shear strength of subgrade soil
- A new correlation is proposed between CBR and shear strength values
- Prediction of CBR using the Hand Vane Shear test and existing correlations
- Comparison between experimental results and existing correlations

### Abstract

In this study, CBR and Shear Vane tests, which are common test methods used in determining the bearing capacity and shear strength of the highway pavement subgrade material, were applied and the effect of the changing water content on the test results was investigated. It is aimed to determine the accuracy of these expressions by obtaining the bearing capacity parameters of the subgrade material with different water contents from laboratory experiments and comparing the results obtained with the empirical expressions in the literature. Shear strength and CBR values of five samples prepared at 15%, 16%, 17%, 18%, and 20% water contents were obtained experimentally. The experimental results obtained and the results calculated using the correlations found in the literature were compared. As a result of the study, the shear strength values obtained from the shear vane test, which is recommended to be preferred in terms of ease of application, were used in the selected correlation relations and CBR values were calculated. By comparing the experimental and calculated CBR values, the approximation accuracies of the existing correlation expressions were presented and it was seen that it was possible to find the CBR value with a maximum accuracy of 90%. In addition, this study presents a new correlation that gives the relationship between shear strength and CBR using the data obtained from the experimental results. With the new equation created; After the shear strength value was obtained experimentally, it was seen that the CBR value could be found with 96% accuracy.

### Information

Received:

03.04.2022

Received in revised:

12.04.2022

Accepted:

12.04.2022

**Keywords:** CBR, shear strength, hand vane shear tester, water content, correlations

### 1. Introduction

In recent years, considering the increase in road construction, the design of road pavements has become a widely studied problem, especially in terms of time and cost. For this reason, the analysis and characterization of the subgrade, which is one of the determining parameters in the characteristics of the pavement, continues to be the area of interest for many researchers [1-3].

The bearing capacity of the subgrade is determined by the California Bearing Ratio (CBR) Test method, which can be performed both in situ and in the laboratory. Determination of the mechanical properties of the subgrade, its bearing capacity, and another important

parameter, the shear strength; Due to the properties of the material, it requires the solution of a problem in which complex behaviours are combined. For this reason, in this study, while determining the bearing capacity of the subgrade with the CBR test method, a second test method, the shear vane test, was applied to determine the shear strength.

In addition to being a test method that is generally applied in the field, the shear vane test has been widely used in recent years due to its ease of application and the fact that laboratory equipment is economical compared to CBR test equipment [4]. In the case of combined stress caused by the anisotropic nature of the subgrade and the loads it is exposed to, it is necessary to know the values

\*Corresponding author: sgokova@mehmetakif.edu.tr (S. Gökova), +90 533 725 7074

that determine its behaviour against shear in calculating the bearing capacity [5]. For this reason, the shear vane test method, which is very convenient to be applied in laboratory conditions, was chosen and the shear strength of the subgrade was found.

Knowing the relationship between shear strength and bearing capacity becomes very important when considering the subgrade, whose properties are defined by the need for many experimental data. For this reason, many researchers have developed correlation expressions that give the relationship between bearing capacity and shear strength [6-8]. The creation of these correlations is very important in terms of easily calculating the sought value in cases where experimental studies cannot be performed. However, considering the subgrade whose behavioural characteristics change depending on many variables, the validity of the correlations requires the selection of the correct correlation and the minimum level of experimental data that can provide confirmation.

Considering that the California bearing ratio (CBR), which is directly related to the bearing capacity of a soil, varies depending on the moisture content and saturation level of the soil [9], 5 soil samples with different water content were tested in this study. Both CBR and shear vane tests of these prepared samples were performed and some of the correlation relations found in the literature and suitable for the material used in the study were selected, and the approximation percentages of the relations were calculated in the light of the experimental data. In addition, it has been seen that the shear vane test method can be used in cases where the CBR test cannot be performed, allowing the CBR value to be found through the relevant correlation relation.

## 2. Existing Correlations

For the design and analysis of road pavements, it is necessary to know the mechanical properties of the subgrade material. For this purpose, correlations between CBR and other soil properties have been developed as an alternative to many material tests by researchers [4,10,11]. Relationships between in-situ or laboratory CBR test and ultimate bearing capacity [9,12], CBR - modulus of elasticity relations [1,13], and CBR-shear strength relations [6,7,14] can be established through widely used correlations as a result of many studies developed and conducted. Therefore, the use of correlation relations developed instead of performing experiments that are difficult and costly in terms of implementation has been preferred by many researchers to determine soil parameters.

Since the soil has many variables due to its material structure, each correlation may not be suitable for a soil sample located in another region. For this reason, researchers working on this subject have carried out

experiments using as many different variables as possible and obtained different correlations. One of the most important variables here; is the limit values of the soil sample studied [15, 16].

Correlations suitable for the classification and limit values of the soil sample used in this study were selected from the literature and these are mentioned below.

The first of the relations chosen is the correlation relation between shear strength and CBR (Equation 1), developed by Black [6] for remolded clay soil and based on the theoretical bearing capacity of the soil.

Giroud and Han [8] worked on the determination of the theoretically developed base layer thickness related to the failure modes of reinforced, unpaved roads and presented the equation given in Equation 2.

In the study by Rushema [16], some of the relationships between shear strength and CBR are discussed on the established accuracy rates. One of the correlation relations in this study, USCOE (US Army Corps of Engineers) was chosen and presented in Equation 3.

The statement developed by Gregory and Cross [7] and based on the theory of bearing capacity equality has been obtained by performing the triaxial shear test and CBR tests for cohesive inorganic soil material (See Equation 4).

$$\text{CBR}=0.043C_u \quad (1)$$

$$\text{CBR}=0.033C_u \quad (2)$$

$$\text{CBR}=0.0087C_u^{1.3723} \quad (3)$$

$$\text{CBR}=0.09C_u \quad (4)$$

The term  $C_u$  in the above equations is shear strength and is expressed in kPa.

## 3. Material and Methods

### 3.1. Material properties

In this study, low plasticity clay material obtained from the Isparta Airport region was used. The results obtained by performing Atterberg limit tests for the classification of this material taken from the subgrade and the material class determined accordingly are presented in Table 1.

As seen in Table 1, it was determined that the soil class of the selected material was low plasticity inorganic clay (CL).

Wet sieve analysis has been performed to determine the granulometry of the material and the results are shown in Table 2 and Figure 1.

Table 1. Subgrade soil Atterberg Limits

Liquid limit	46%	(TS 1900-1 AASHTO T-89)
Plastic limit	17%	(TS 1900-1 AASHTO T-90)
Plastic index	29%	(PI = LL - PL)
Soil classification	CL	Unified Soil Classification

Table 1. Sieve analysis results of subgrade soil (ASTM D1140).

Sieve No	Sieve Opening (mm)	Percent Passing (%)
3/8"	9.53	100.00
No 4	4.760	99.48
No 10	2.000	99.18
No 40	0.425	94.93
No 200	0.075	56.35

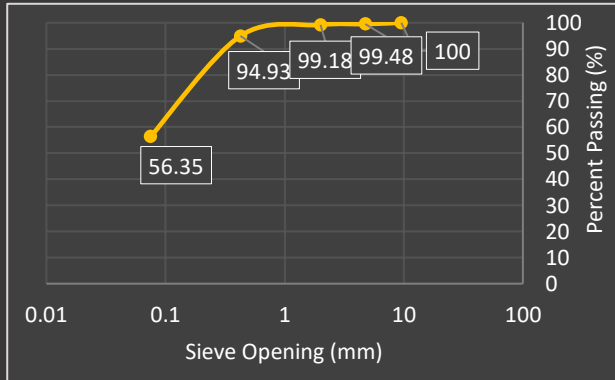


Figure 1. Granulometry curve of subgrade material

To determine the optimum water content of the material used in the tests, the Proctor test was performed and the dry unit weights ( $\gamma_k$ ) at different water contents ( $\omega$ ) were determined (Figure 2).

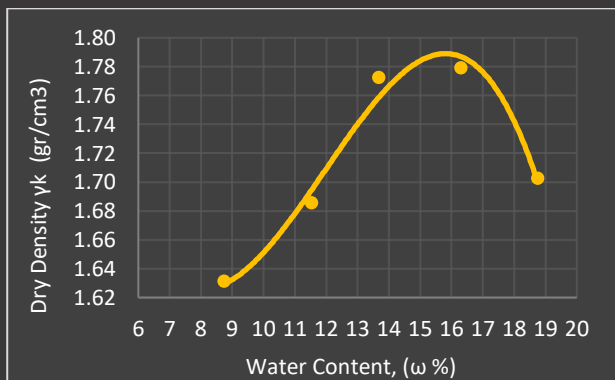


Figure 2. Moisture content-dry density relationship from standard Proctor tests

The results obtained from the Proctor test were taken into account while determining the water content of the samples that were subjected to CBR and shear vane tests.

### 3.2. Test Methods

In this study, two different test methods, CBR and shear vane test were used to determine the bearing capacity and shear strength of the soil sample at different water contents.

#### 3.2.1. CBR (California bearing ratio) test

The CBR test is used to evaluate the bearing capacity of the subgrade, base and subbase layer materials in the road pavement. CBR is a test method that gives the ratio of the bearing capacity of the material to the bearing capacity of the standard crushed stone as a percentage [17].

Determining the CBR value in a construction zone requires a lot of effort in terms of sample supply. In addition, to carry out the test in a laboratory environment, it is necessary to know the soil class of the material and the parameters such as optimum water content. To determine these parameters, a series of pre-tests are required. All these situations create a disadvantage in terms of time and cost [18]. CBR test is a common test method that gives reliable results in the bearing capacity calculation. However, the disadvantages mentioned above have revealed the need to find alternative methods to CBR testing.

In this study, the above-mentioned preliminary experiments were carried out to perform the CBR test and the relevant parameters were obtained. Samples prepared in five different water contents were compressed into CBR molds by ASTM D1883-16 standard and tests were carried out (Figure 3).



Figure 3. Automatic CBR test machine

#### 3.2.2. Hand vane shear test

This test method can be used in the field directly on the ground or in the laboratory on specimens compressed into molds to certain standards. The hand vane shear tester is a simple and portable test kit (ASTM D8121/D8121M-19) for measuring the undrained shear strength of saturated, fine-grained, cohesive soils. The method of obtaining the results found with this device; may differ according to the calculation methods of the companies producing the hand vane shear test device. This test method is very easy to perform and the equipment costs are more economical compared to the CBR test [16]. In addition, in terms of applicability, the

shear vane test can be performed in a shorter time than the CBR test method [19,20].

The device (Geonor-H-60 Hand Vane Tester) used in this study can directly give the shear strength of the material in pascal. There are 3 different diameter torque blades in the test kit, which can be measured in 3 different strength ranges (Figure 4). The torque blade was selected depending on the rigidity of the sample to be tested, and tests were carried out by the ASTM D8121/D8121M-19 standard on the samples that were compressed into the CBR mold.



Figure 4. Hand vane shear tester

It is known that the shear vane test is a test method that can be applied to soft ground materials [21]. On the other hand, in the study, preliminary tests were carried out on samples with a water content lower than the optimum value. However, since healthy measurements could not be made, the results of the pre-trial test were not included in this study.

#### 4. Results and Discussions

In this study, the results obtained from two separate experiments with different water contents are presented in this section. Then, the relationship between two separate parameters obtained from the experiments was expressed as a correlation. In addition, CBR values obtained from 4 different correlation relations and experimental results are compared and presented below as a graphic and table.

##### 4.1. Laboratory test results

The CBR and shear vane tests performed in the laboratory were performed for each of the 5 samples with different water content, and the changes in the bearing capacity and shear strength values according to the water content are presented in Figure 5 and Figure 6, respectively. In addition, in Table 3, percentage changes in CBR and shear strength results according to water content are shown.

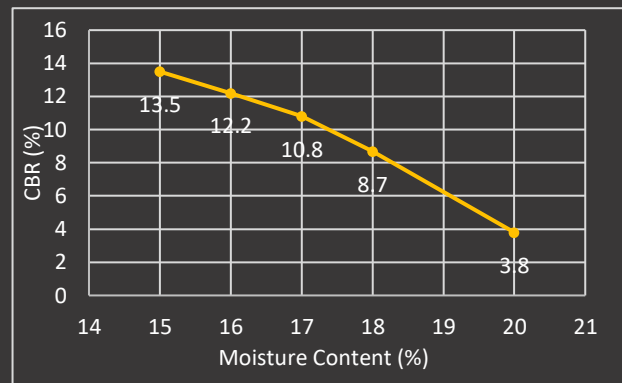


Figure 5. Moisture Content vs. CBR values

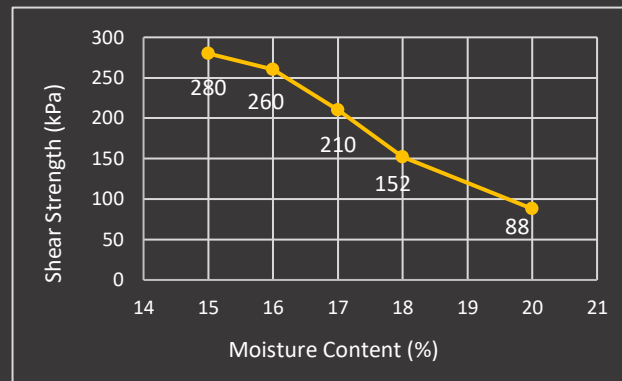


Figure 6. Moisture Content vs. Shear Strength

In the graphs given in Figures 5 and 6, CBR and shear strength values decrease with exceeding the optimum content. Due to the mineralogical structure of the clay, as the water content increases, the distance between the grains increases, and the attractive forces decrease.

Table 3. Tendencies to decrease in  $C_u$  and CBR values according to water content.

Water Content (%)	CBR (%)	Shear Vane Test	$C_u$ Decreasing Trend (%)	CBR Decreasing Trend (%)
15	13.5	280	7.14	9.63
16	12.2	260	19.23	11.48
17	10.8	210	27.62	19.44
18	8.7	152	42.11	56.32
20	3.8	88	-	-

As can be seen from the experimental results and percentages of change given in Table 3, as the water content increases, the CBR and shear strength decrease, and the rate of decrease of the values increases after the optimum water content is exceeded. This behavior is also consistent with the results of the Proctor test presented in Figure 2.

To determine the relations between the data obtained by the two test methods, the values in the same water contents were compared and the changes in the values obtained from the CBR and shear vane tests in the same water contents were presented in Figure 7.

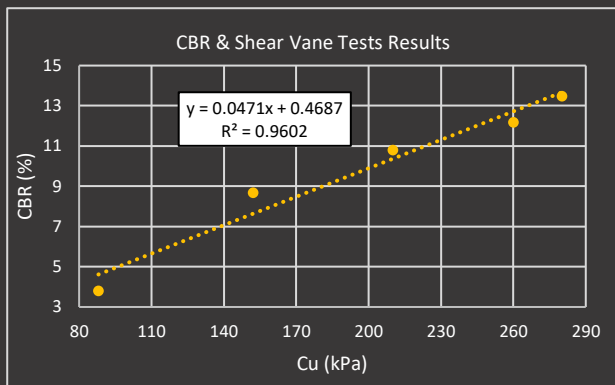


Figure 7. CBR vs Shear Strength

The correlation between the experimental results presented in Figure 7 was established using a linear equation and this correlation was expressed with the function given in Equation 5.

$$CBR = 0.0471 \cdot C_u + 0.4687 \quad (5)$$

The R-squared value, which expresses the compatibility of the linear function with the experimental results, was found to be 0.9602. This value shows that the proposed linear relationship can be used to calculate the corresponding values for similar subgrade materials.

#### 4.2. The Existing Correlation Results

CBR values were calculated by using the shear strength result values obtained using the hand shear vane test kit in the laboratory and the equations given in the existing

correlation section. The results obtained from the CBR and shear vane tests and equations performed at different water contents are presented in Table 4. In Figure 8, the CBR values obtained from the equations and experiments are shown comparatively.

According to the numerical results presented in Table 4, it is seen that Equation 1 gives the closest result to the experimental results among 5 samples. Accordingly, the closest values were seen in sample 5, the experimental and correlated CBR values were found to be 3.8 and 3.79, respectively.

When the results given in Table 4 and Figure 8 are examined, it is seen that the closest CBR value to the results of the experimental study was obtained with Equation 1 suggested by Black [6]. In addition, it was observed that the other two relations gave very close results at low CBR values. It has been seen that the equations giving the highest and lowest values out of the four selected equations are Equation 4 and Equation 2, respectively, which is important in terms of determining the limit values.

#### 5. Conclusions

In this study, two different test methods were applied to determine the design parameters of the cohesive fine-grained subgrade material. For each test, samples with 5 different water contents were tested and the selected water contents were determined by considering the results of the Proctor test.

Table 4. CBR values from experiments and correlations

Sample No	Moisture Content (%)	Cu (kPa) (Exp)	CBR (From Correlations)				CBR (%) (Exp)
			Eq-1	Eq-2	Eq-3	Eq-4	
1	15	280	12.04	9.24	19.85	25.2	13.5
2	16	260	11.18	8.58	17.93	23.4	12.2
3	17	210	9.03	6.93	13.38	18.9	10.8
4	18	152	6.54	5.02	8.58	13.68	8.7
5	20	88	3.79	2.90	4.05	7.92	3.8

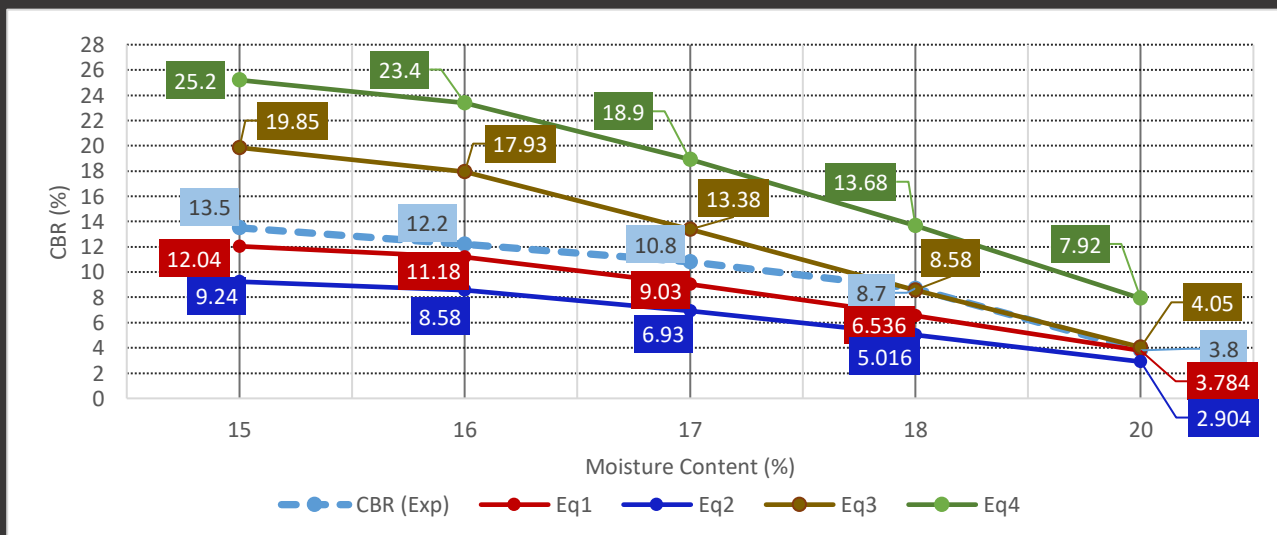


Figure 8. Comparison between correlated and experimental CBR values

In addition, since the CBR and shear vane test methods will be associated in the study, the applicability of the shear vane test on soft soil material has been decisive in the selection of values above the optimum value. As expected in the test results, it was observed that CBR and shear strength values decreased as the water content increased, and there was a significant decrease in both values (CBR and Cu), especially at rates above 18% water content.

In addition, in this study, a new equation is proposed by establishing a linear relationship between the experimentally obtained CBR and shear strength results. Using this new proposed equation, the CBR value can be found with 96% accuracy after the shear strength of the CL type subgrade material is obtained experimentally.

In the next stage of the study, CBR values were calculated by using the results obtained from the shear vane test in 4 different correlation relations found in the literature. The approximation tendencies of the selected correlation relations were determined by comparing the calculated values with the experimental results. Thus, in cases where it is not possible to perform the CBR test, it has been determined that the shear vane test, which is easier and less costly in terms of application, can be performed as an alternative. It has been seen that it is possible to calculate the CBR value with 90% accuracy by using the obtained shear strength values in the correlation expression (Equation 1), the accuracy of which was determined as a result of the study. These results provide a fast, reliable, and economical method to determine the bearing capacity of the subgrade, which is one of the important parameters in pavement design.

#### Declaration of Interest Statement

The author declare that they have no known competing financial interests or personal relationships that could have appeared to influence the work reported in this paper.

#### References

- [1] Brown, S. F., O'Reilly, M. P., & Loach, S. C. (1990). The relationship between California Bearing Ratio and elastic stiffness for compacted clays. *Ground Engineering*, 23(8).
- [2] Frost, M. W., Fleming, P. R., & Rogers, C. D. (2004). Cyclic triaxial tests on clay subgrades for analytical pavement design. *Journal of transportation Engineering*, 130(3), 378-386. [https://doi.org/10.1061/\(ASCE\)0733-947X\(2004\)130:3\(378\)](https://doi.org/10.1061/(ASCE)0733-947X(2004)130:3(378))
- [3] Roy, T. K. (2013). Influence of sand on strength characteristics of cohesive soil for using as subgrade of road. *Procedia-Social and Behavioral Sciences*, 104, 218-224. <https://doi.org/10.1016/j.sbspro.2013.11.114>
- [4] EL-Sherif, M. M., (1996). Correlation between California Bearing Ratio and Shear Strength Measurement of Soil. *Engineering Research Journal*, 47, 261-269.
- [5] Kirkgard, M. M., & Lade, P. V. (1991). *Anisotropy of normally consolidated San Francisco bay mud*. ASTM International.
- [6] Black, W. P. (1979). The strength of clay subgrades: its measurement by a penetrometer.
- [7] Gregory, G. H., & Cross, S. A. (2007). Correlation of California bearing ratio with shear strength parameters. *Transportation research record*, 1989(1), 148-153. <https://doi.org/10.3141/2F1989-17>
- [8] Giroud, J. P., & Han, J. (2004). Design method for geogrid-reinforced unpaved roads. II. Calibration and applications. *Journal of Geotechnical and Geoenvironmental Engineering*, 130(8), 787-797. [https://doi.org/10.1061/\(ASCE\)1090-0241\(2004\)130:8\(787\)](https://doi.org/10.1061/(ASCE)1090-0241(2004)130:8(787))
- [9] Black, W. P. M. (1962). A method of estimating the California bearing ratio of cohesive soils from plasticity data. *Geotechnique*, 12(4), 271-282. <https://doi.org/10.1680/geot.1962.12.4.271>
- [10] Purwana, Y. M., & Nikraz, H. (2014). The correlation between the CBR and shear strength in unsaturated soil conditions. *International Journal of Transportation Engineering*, 1(3), 211-222. <https://dx.doi.org/10.22119/ijte.2014.4790>
- [11] Reddy, S., Ruchita, N., Sharma, P. & Satyanarayana, S.V. (2019). Prediction of California Bearing Ratio through Empirical Correlations of Index Properties for Tropical Indian Soils. *International Journal of Innovations in Engineering and Technology*, 15(1), 67-77. <http://dx.doi.org/10.21172/ijiet.151.09>
- [12] Razouki, S. S., Kuttah, D. K., Al-Damluji, O. A., & Nashat, I. H. (2005). Strong correlation between the bearing capacity and CBR of a gypsiferous subgrade soil subjected to long-term soaking. In *Proceedings of the international conferences on the bearing capacity of roads, railways and airfields*.
- [13] Narzary, B. K., & Ahamad, K. U. (2018). Estimating elastic modulus of California bearing ratio test sample using finite element model. *Construction and Building Materials*, 175, 601-609. <https://doi.org/10.1016/j.conbuildmat.2018.04.228>
- [14] Joseph, D., & Vipulanandan, C. (2010). Correlation between California bearing ratio (CBR) and soil parameters. *J. CIGMAT. Geotechnical Research*, 31, 44-9.
- [15] Shimobe, S., & Spagnoli, G. (2020). Relationships between undrained shear strength, liquidity index, and water content ratio of clays. *Bulletin of Engineering Geology and the Environment*, 79(9), 4817-4828. <https://doi.org/10.1007/s10064-020-01844-5>
- [16] Rushema, B. W. (2021). Examination of the Correlation between Shear Strength, California Bearing Ratio, and Index Properties of Fine-grained Soil. *Master of Science in Civil Engineering Theses, Kennesaw State University, Georgia, USA*
- [17] Caicedo, B., & Mendoza, C. (2015). Geotechnical behaviour of unpaved roads: understanding the CBR test. *From Fundamentals to Applications in Geotechnics*, 95-100. <https://doi.org/10.3233/978-1-61499-603-3-95>
- [18] Şeker, V., & Selçuk, L. (2018). Kaliforniya taşıma oranının laboratuvar değerlerinin belirlenmesinde P-dalga hızının kullanılabilirliği. 71. *Türkiye Jeoloji Kurultayı*.
- [19] Ullah, A. (2017). Application of vane shear tools to assess the shear strength of remolded clay soil. *Research Journal of Engineering*, 6(1), 1-4.
- [20] Arslan, E., Düzen, İ., Develioglu, I., & Pulat, H. F. (2021). Undrained shear strength of polypropylene fiber

reinforced alluvial clay. *Environmental Research and Technology*, 4(3), 219-229.  
<https://doi.org/10.35208/ert.903408>

- [21] Ayadat, T. (2021). Determination of the Undrained Shear Strength of Sensitive Clay Using Some Laboratory Soil Data. *Studies in Engineering and Technology*, 8(1), 14-27.  
<https://doi.org/10.11114/set.v8i1.5149>



## Effects of waste engine oil and crumb rubber rejuvenator on the performance of 100% RAP binder

Ahmed Eltwati<sup>a</sup>, Mahmoud Enieb<sup>b</sup>, Saleh Ahmeed<sup>c</sup>, Zaid Al-Saffar<sup>d</sup>, Azman Mohamed<sup>e</sup>

<sup>a</sup>Department of Roads and Airports Engineering, Bright Star University, Brega, Libya

<sup>b</sup>Department of Civil Engineering, Assiut University, Assiut, Egypt.

<sup>c</sup>Department of Roads and Airports Engineering, Bright Star University, Ajdabiya, Libya

<sup>d</sup>Department of Building and Construction Engineering, Northern Technical University, Iraq.

<sup>e</sup>School of Civil Engineering, Universiti Teknologi Malaysia, Johor, Malaysia

### Highlights

- Hybrid rejuvenator with CR and WEO was used to restore the aged binder
- Adding 100% RAP increased the stiffness and rutting resistance
- Proper use of WEO-CR rejuvenator enhanced the performance

### Abstract

It is frequently essential to add rejuvenators to recycled mixtures comprising reclaimed asphalt pavement (RAP) to increase their performance. In this research, CR was desulfurized using WEO to produce a compound rejuvenator. The asphalt mixes containing 100% RAP binder were modified and rejuvenated with 0%, 3%, 6%, 9%, and 12% WEO-CR. The performance of the HMA samples were assessed using the Marshall stability-flow test, indirect tensile strength (ITS) test, and wheel-tracking device. The results showed that using a 9% WEO-CR rejuvenator restores the physical properties of the aged binder. In addition, the findings revealed that adding 100% RAP binder to the asphalt mixtures increased the tested properties of HMA samples; however, for the long-term performance of HMA, the aged binder may adversely affect the performance of the HMA mixture. Therefore, the addition of the WEO-CR rejuvenator was found to improve the overall performance of the mixture which improved the physical and chemical properties of the asphalt binder and enhanced the mechanical performance of HMA compared to the control mixture.

### Information

Received: 13.02.2022  
 Received in revised: 05.04.2022  
 Accepted: 05.04.2022

**Keywords:** aged binder, crumb rubber, RAP, rejuvenator, waste engine oil

### 1. Introduction

Using reclaimed asphalt pavement (RAP) in hot-mix asphalt (HMA) helps to reduce the overall cost of project, material transportation expenses, and also protects the environment [1]. As a result of the milling, RAP includes aggregate that is much finer than virgin aggregate. This issue may be solved by dividing the RAP into multiple sizes. Furthermore, the RAP binder is very stiff, resulting in mixes with undesirable cracking and workability properties at a lower temperature [2-3]. Therefore, Scientists have attempted following approaches such as soft asphalt binder, warm mix asphalt (WMA) additives, and recycling agents to address these issues [4-6]. In general, all these approaches may be recognized as

recycling agents. The recycling agents act as softeners to decrease the impacts of the high stiffness of the aged binder and enhance its workability, or as rejuvenators to lessen the stiffness of the aged binder by halting the aging process, improving workability and mitigating cracking possibility [7].

The inclusion of some waste materials in any of the aforementioned procedures helps ensuring the long-term durability of the pavement. To increase the performance of the reclaimed binder, several rejuvenators have been applied. The disposal of waste engine oil (WEO) was extremely crucial as most states create substantial volumes of WEO annually [8]. The use of WEO as an asphalt rejuvenator was very beneficial, and other

\*Corresponding author: [ahmed.eltwati@bsu.edu.ly](mailto:ahmed.eltwati@bsu.edu.ly) (A. Eltwati), +218913761046

investigations have demonstrated that WEO has a great rejuvenation function [9-11]. Furthermore, WEO has a flash point of above 220 degrees Celsius, indicating that it is stable sufficient to be used in hot asphalt mixes [12]. However, the acidity and viscosity of WEO have a major concern of the rejuvenation process [13], therefore quality control in WEO is a critical issue [14]. Furthermore, the WEO-rejuvenated binders revealed a significant moisture sensitivity due to weak adhesion [15].

The adhesion of crumb rubber (CR) and asphalt binder are excellent [16-18]. The CR increases the elastic properties of asphalt mixes incorporating RAP and also keeping costs down [19]. On the other side, the inclusion of CR to asphalt mixes incorporating RAP has a negative influence on moisture susceptibility [20-21]. Furthermore, the rubber molecules do not mix well with the aged binders [22]. Incompatibility and deposition of rubber molecules are caused by variations in molecular size, polarity, and solubility between rubber and aged asphalt binder [23]. Lin et al. [24] reported that asphalt binders with a higher aromatic component liquefy more CR than an asphalt binder with a lower aromatic fraction. Compared with virgin asphalt binder, aged asphalt has fewer aromatic components [25]. Therefore, the compatibility of rubber with the aged binder has deteriorated. As a result, when CR is incorporated into an aged binder, the compatibility must be improved.

This paper intends to produce a CR and WEO rejuvenator to alleviate the difficulties described earlier and enhance the performance of mixtures comprising 100% RAP binder. The purpose of this study was to identify the optimum recycling agent dose in order to achieve the best performance of high-RAP mixes. The CR was implemented in this research to mitigate the reduction in rutting resistance caused by the addition of WEO. The objectives of this research were to evaluate the influence of compound rejuvenator (CR-WEO) on the physical and chemical properties of aged binder. In addition, the Marshall test, indirect tensile strength (ITS), and wheel-tracking test were performed to assess the mechanical properties of HMA samples. Finally, a cost analysis was carried out to assess the cost of HMA containing WEO-CR in comparison to the conventional HMA.

## 2. Materials and Sample Preparation

### 2.1. Materials

#### 2.1.1. RAP binder

The RAP binder was recovered by melting it in methylene as stated by ASTM D2172 and afterward reclaiming it utilizing a rotary evaporator according to ASTM D5404. Before batching, all extracted binders were mixed to achieve consistent characteristics in the RAP binder. The RAP binder's performance grade (PG) was determined to be 94 and -4 °C. The RAP binder content was found to be

5.72 percent. Table 1 shows the characteristics of the RAP binder used in this study. The findings of physical testing of RAP demonstrate that it has a stiff character. The low penetration and ductility values demonstrate this.

Table 1. Physical properties of aged binder.

Property	Value	Specification	Standards
Penetration at 25°C, 5s, (0.1 mm)	14.8	60-70	ASTM D5-20 [26]
Softening point (°C)	75.9	48-52	ASTM D36-14 [27]
Ductility at 25°C, (cm)	9.7	>100	ASTM D113-17 [28]
Flash point (°C)	75.9	48-52	ASTM D36-14 [27]
Specific gravity	1.07	1.0-1.05	ASTM D70-21 [29]

#### 2.1.2. Aggregates

Limestone aggregate was used as the virgin natural aggregate in this investigation. Table 2 shows the gradation of aggregate, and the prescribed gradation was following ASTM D3515.

#### 2.1.3. Crumb rubber (CR)

CR with a maximum particle size of 0.157 mm (#80) was used for this experiment. It's important to mention that the CR was obtained from end-of-life tires using an ambient process.

#### 2.1.4. Waste engine oil (WEO)

The WEO employed in this investigation was a 4,000-kilometer-use synthetic 5W20 gasoline oil. WEO had a kinematic viscosity of 0.041 Pas (ASTM D-4402) at 135 °C and a flash point of 265 °C (ASTM D-92).

### 2.2. Preparation of WEO-CR rejuvenator

WEO was initially heated at approximately 170 °C. The CR was gently combined with the WEO and sheared at 5000 rpm for 60 mins [30]. The percentage of WEO and CR of total weight of the compound rejuvenator was estimated to be 77% and 23%, respectively. Numerous samples having varying percentages of WEO and CR were examined by a trial-and-error procedure to determine the correct WEO-CR ratio. The production process of the WEO-CR rejuvenator is shown in Figure 1.

Table 2. Gradation of aggregates and specification

Sieve size	Passing%	Specification
25.40 mm	100	100
12.50 mm	92.4	80-100
9.50 mm	72.6	60-80
4.75 mm	50.3	48-65
2.38 mm	39.7	35-50
0.60 mm	25.5	19-30
0.30 mm	16.8	13-23
0.150 mm	8.2	7-15
0.075 mm	4.9	3-8

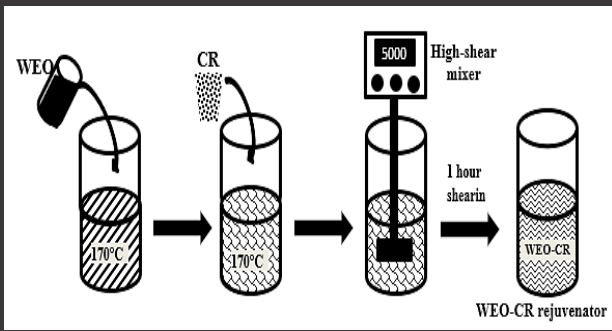


Figure 1. Process of production of WEO-CR rejuvenator.

**2.3. Preparation of rejuvenated binder samples**

To prepare the rejuvenated binders, the 100% RAP binder content was heated up to 140 °C before being combined with the rejuvenated WEO-CR for 15 minutes in a high-shear blender at 1000 rpm. The WEO-CR rejuvenator was mixed with the RAP binder at various doses (3%, 6%, 9%, and 12% by weight of the RAP binder). Figure 2 shows the production process of rejuvenated asphalt binder samples.

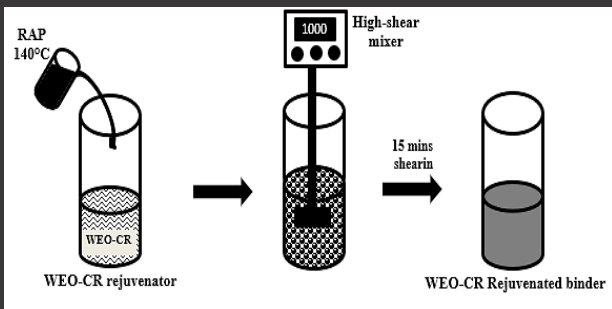


Figure 2. Process of production of the rejuvenated binder.

**2.4. Preparation of asphalt mixtures**

At 163 °C, rejuvenated binders comprising 100% RAP were mixed with natural limestone aggregate with a maximum nominal size of 12.5 mm (ASTM D2493). The mixture was left to cool down to a compaction temperature of 153 °C (ASTM D2493). The Marshall mix design showed that the optimum bitumen content was 6.02 % which achieved 4.0 % air voids in the overall volume of the mixtures. The optimum asphalt content and the volumetric properties for all HMA samples are shown in Table 3.

Table 3. Optimum asphalt content and volumetric properties of each mixture type.

Mixture type	Volumetric properties		
	Optimum asphalt content %	Total voids in mixture %	Density (gm/cm <sup>3</sup> )
Control Mix	6.02	4.00	2.43
100%RAP	6.02	3.94	2.45
100%RAP+3%WEO-CR	6.02	4.02	2.46
100%RAP+6%WEO-CR	6.02	4.05	2.44
100%RAP+9%WEO-CR	6.02	4.06	2.43
100%RAP+12%WEO-CR	6.02	4.10	2.42

**3. Methods**

**3.1. Temperature susceptibility assessment**

Penetration index (PI) and penetration viscosity number (PVN) methods were used in this study to evaluate the effect of WEO-CR addition on the temperature susceptibility of rejuvenated asphalt binders. The Shell Bitumen Handbook [31] shows how to calculate PI using a traditional technique, as shown in Equation 1 beneath. Using the results of penetration and viscosity experiments, the PVN method is used to assess the temperature susceptibility of binders. Equation 2 [32] is used to calculate PVN.

$$PI = \frac{1950 - 500 \times \log(\text{Pen}) - 20 \times SP}{50 \times \log(\text{Pen}) - SP - 120} \tag{1}$$

$$PVN = 1.5 \times \left( \frac{4.258 - 0.7967 \times \log(\text{Pen}) - \log(V)}{0.7951 - 0.1858 \times \log(\text{Pen})} \right) \tag{2}$$

Where;

Pen denotes the penetration at 25°C,  
 SP denotes the temperature of softening point,  
 V denotes the viscosity at 135°C in centistokes.

It should be stated that the low-temperature cracking is more likely in asphalt mixes consisting of binders with low PI values. Most acceptable paving binders have PI values from +1.0 to -1.0. In terms of the temperature sensitivity of binders, higher PI values indicate greater performance. On the other side, PVN values for asphalt binders typically range from +0.5 to -2.0 [32]. The temperature sensitivity of the binder increases as the PVN value decreases.

**3.2. Marshall test**

Marshall testing is used to determine the appropriate asphalt composition as well as the mixture's properties. This test is performed to measure the stability of the asphalt mixture and the deformation (flow). The capability of asphalt mixes to tolerate loads up to plastic discharge is indicted by stability. The load causes a change in form until it approaches the collapse limit, which is known as flow.

**3.3. Indirect tensile strength test**

The Indirect Tensile Strength test of asphalt mixes is performed by applying a load vertically to the cylindrical specimen's diameter at a specified rate of deformation and temperature. The highest load at the time of failure is utilized to calculate the indirect tensile strength of asphalt mixture. This experiment is also used to assess the quality of the asphalt mixture and to detect the possible water damage when the test results are acquired from separate specimens, especially when the test specimen is submerged and not soaked. This test was carried out at 25 °C according to the ASTM D6931-2017 [33].

### 3.4. Wheel-Track testing

The wheel tracking device is conducted to measure the resistance of asphalt mixtures to deformation of the wheel path, it also simulates traffic loads or vehicle wheel load on the asphalt surface until deformation occurs in the wheel path. Wheel path deformation is common on asphalt pavements, particularly in tropical regions. In this experiment, the HMA sample tests were tested at 50°C. The instrument has a wheel load of 0.705 kN and travels across the HMA sample's surface to make 10,000s passes. This test was run per the AASHTO T324-11 [34].

## 4. Results and Discussion

### 4.1. Physical properties of asphalt binder samples

Figures 3, 4, and 5 depict the penetration, softening point, and ductility of the virgin, RAP, and rejuvenated binder specimens. It can be observed, adding the RAP binder to a virgin binder enhances the stiffness, which makes the binder less susceptible to temperature owing to a the higher asphaltene content. Furthermore, the aromatics in the WEO-CR rejuvenator led to the development and incorporation of the asphaltene diffusion medium, which acts as a lubricant in the colloidal structure [15]. As a consequence, aromatics can reduce viscosity and soften asphalt binders. Furthermore, lowering the aromatic dosage reduces the penetration and ductility while increasing the softening point in virgin asphalt binder integrating RAP binder. Nevertheless, the characteristics of the RAP binders can be improved by utilizing the WEO-CR rejuvenator. WEO-CR rejuvenator can reduce the aging impact of RAP binders by decreasing the stiffness caused by oxidation and the interaction of the binder polar molecules. Further, the addition of the WEO-CR rejuvenator to the RAP binder increased penetration and ductility while decreasing softening point, shown in the figures, and the effects were more pronounced as the WEO-CR rejuvenator concentration increased. It can also be observed that the 9% content of WEO-CR yielded the optimum content that can restore the properties of the aged binder.

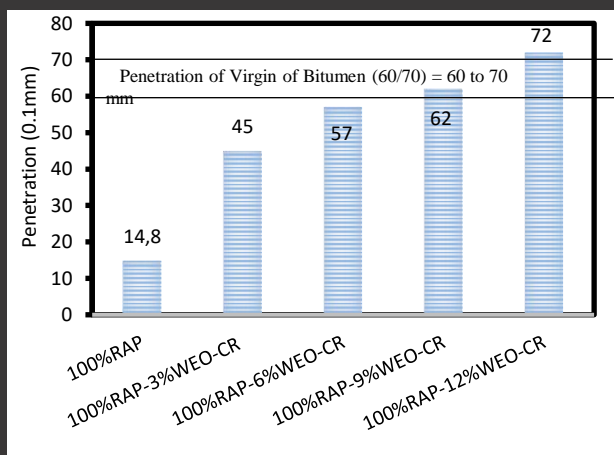


Figure 3. Penetration values of asphalt binder samples.

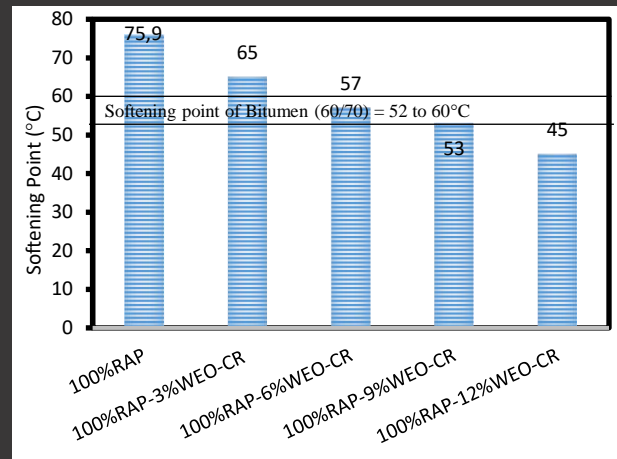


Figure 4. Softening point values of asphalt binder samples.

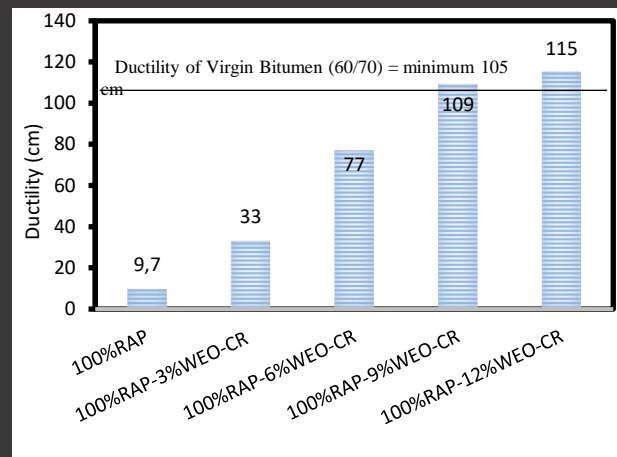


Figure 5. Ductility values of asphalt binder samples.

### 4.2. Temperature susceptibility assessment

Table 2 shows the PI and PVN values for the virgin, RAP, and rejuvenated binders. The results showed that the 100% RAP binder had the lowest values for PI and PVN, indicating that this binder is brittle, susceptible to cracking in cold climates, and rutting in hot climates. Furthermore, at 135°C, such binders have a low viscosity, which lead to tender mix issues (like instability, distortion, and rutting) during compaction under traffic loads [35]. On the other side, Table 4 exhibits that the RAP binders containing 3%WEO-CR and 6%WEO-CR had the highest values of PI and PVN, respectively. This indicates that these binders are the least susceptible to temperature.

Table 4. PI and PVN values of asphalt binder samples.

Asphalt type	PI	PVN
Virgin binder	+0.29	-0.18
100%RAP	-0.59	-0.21
100%RAP+3%WEO/CR	<b>+0.38</b>	+0.14
100%RAP+6%WEO/CR	+0.20	<b>+0.23</b>
100%RAP+9%WEO/CR	+0.34	-0.08
100%RAP+12%WEO/CR	+0.16	-0.18

### 4.3. Marshal stability and flow

The results of Marshall stability and flow of virgin, RAP, and rejuvenated HMA samples are shown in Figure 6 and Figure 7, respectively. Both graphs indicated that the RAP caused an increase in instability and a decrease in flow with the addition of a 100% RAP binder. This shows that RAP can boost the loading efficiency and the deformation resistance of the asphalt mixture. The enhancement was attributed to the brittle nature of the RAP, but it should be highlighted that it could be detrimental for asphalt mixtures at low and intermediate temperatures. Nevertheless, the finding is in agreement with the study of Moghadas et al. [36].

The addition of the WEO-CR rejuvenator also seems to have positively influenced the specimens' performance as shown in Figure 4 and Figure 5. This could be due to the higher elasticity of the compound rejuvenator when compared to the conventional mix, which also means that the rejuvenated HMA mixture can sustain higher loading and better resistance to deformation (flow). However, it is worth noting that, even with an increase in the content of the WEO-CR rejuvenator, the addition of RAP had increased the stability and decreased the flow of HMA samples, this is the main benefit of incorporating RAP into asphalt mixtures.

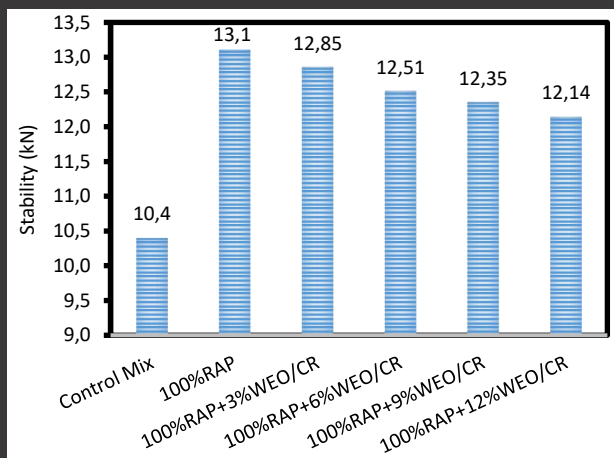


Figure 6. Stability of HMA samples.

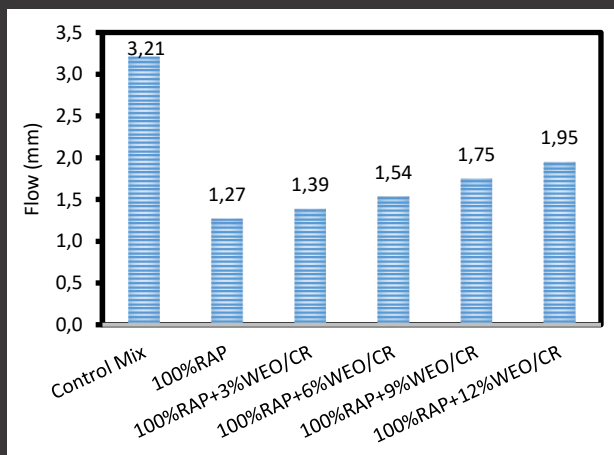


Figure 7. Flow values of HMA samples.

### 4.4. ITS of HMA samples

The HMA samples for the ITS test were produced with 4% voids, and the experiment was carried out following AASHTO T283. Figure 8 depicts the ITS results at 25 °C, where the ITS for the asphalt mixture incorporating 100% RAP was 2 times greater than the control mix (virgin mixture). The greater the ITS value, the stiffer and more viscous the RAP asphalt binders are. This finding is comparable to that of Eltwati et al. [37], who determined that RAP had a considerable influence on ITS, with larger RAP concentrations producing higher ITS values.

It can also be seen that the addition of a compound rejuvenator decreased the ITS values of HMA samples. The increases in the content of WEO-CR led to decrease ITS values of mixtures. This indicates that the rejuvenator decreased the ITS value by lowering the viscosity of the aged asphalt binder in the RAP. However, the ITS value of rejuvenated HMA samples was higher than the control mix (925 kPa). This conclusion was congruent with the findings of Eltwati et al. [38], who observed that the waste engine oil lowered the ITS value.

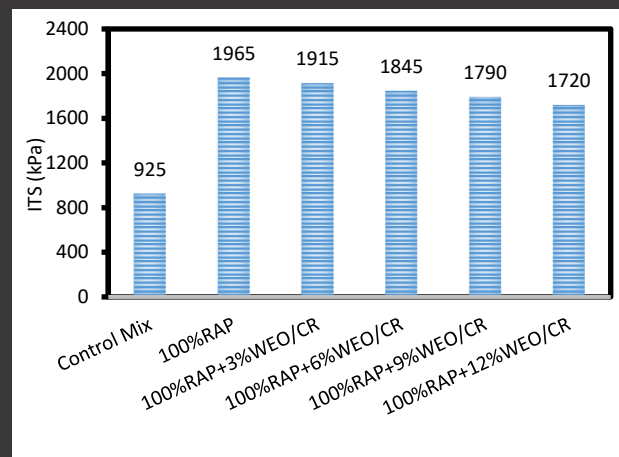


Figure 8. ITS of HMA samples.

### 4.5. Rutting resistance of HMA samples

Figure 9 illustrates that adding 100%RAP binder to the asphalt mixture increased the rut resistance of HMA samples. Rut depths was 0.91 mm for asphalt mixes containing 100% RAP. Because of the substantial amounts of carbonyl molecule in the RAP binder, the HMA samples containing 100% RAP had the lowest rut depth compared to all other HMA samples. This behavior is similar to the observations of Enieb et al. [39], who reported that high amounts of carbonyl in the aged binder lowered rutting depth.

It can be observed that the inclusion of the WEO-CR rejuvenator reduced the rut resistance of HMA samples. In addition, the increase in the amount of rejuvenator into asphalt mixtures led to increase in the rut depth of the sample. The content of the 12%WEO-CR rejuvenator had the highest rut depth compared to other samples. This

finding is in line with the findings of Eltwati et al. [37], who determined that rutting resistance of WEO-rejuvenated mixtures was better than the conventional mixture. The reduction in rut resistance for asphalt mixes containing 100% RAP and rejuvenator was caused by the WEO, which softened the RAP mixture.

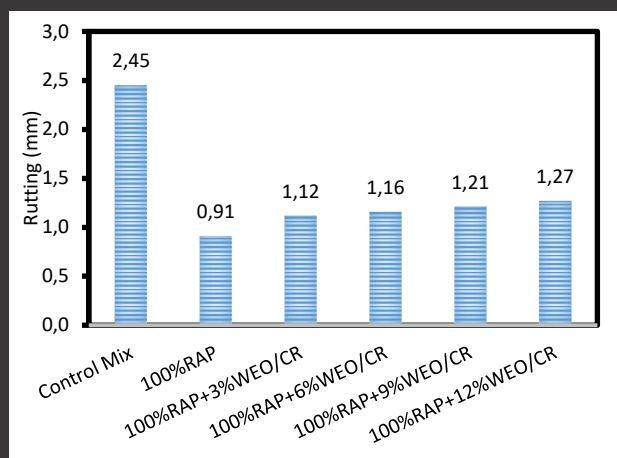


Figure 9. Rutting resistance of HMA samples.

#### 4.6. Cost analysis

The cost of recycled HMA mixes containing WEO and CR was determined using cost analysis. Materials, plant production, transportation, and processing were the most important cost components identified by a previous study [40] for asphalt manufacture. Materials are the most expensive component, accounting for 70% of the total cost of HMA production [41]. Only materials like virgin aggregates, asphalt binder, RAP, WEO, and CR were priced in this analysis according to their usual pricing. Table 5 shows production costs per kg of HMA based on the virgin mixture and 100RAP+9%WEO/CR data. Because of the inclusion of RAP and WEO-CR in the mix, the price of asphalt mixes was reduced by 37.50 percent. The rejuvenated mixture (100RAP+9WEO-CR) is priced \$26.76/ton, while the control Mix is priced at \$42.85/ton, on the cost assessment. 100%RAP, on the other side, is significantly less expensive than a control Mix. However, due to their stiffness, which creates durability concerns, they cannot be included in the road surface, particularly as they aged.

Table 5. Cost analyses of asphalt mixture samples.

Materials	Price (\$/kg)	Control Mix	100% RAP	100RAP+9WEO/CR
Virgin binder	0.48	23.85	-	-
Virgin aggregates	0.02	19.00	-	19.00
RAP binder	0.006	-	6.00	6.00
WEO	0.20	-	-	1.39
CR	0.18	-	-	0.37
Total cost (\$/ton)	-	42.85	6.00	26.76

#### 5. Conclusion

The current study used a research strategy that included a series of physical and chemical experiments to investigate the impacts of the WEO-CR on the characteristics of aged asphalt. In addition, the mechanical characteristics of HMA samples were tested. Based on the findings of the empirical investigation and subsequent discussions, a number of conclusions were established.

- The physical assessment of asphalt binder samples showed that the rejuvenator restored the properties of the aged binder, bringing them closer to the virgin binder. (60/70 penetration grade).
- The temperature susceptibility evaluation of binder samples showed that 100% RAP binder was susceptible to temperature variations. However, the incorporation of the content of 6.0 to 9.0% of WEO-CR to the aged binder improved the temperature susceptibility of the binder sample.
- WEO-CR was shown to improve RAP mixture performance in terms of Marshall tests, ITS, and rutting resistance. The performance of rejuvenated mixtures was even better than the virgin mixture.

#### Declaration of Interest Statement

The authors declare that they have no known competing financial interests or personal relationships that could have appeared to influence the work reported in this paper.

#### Author Contribution Statement

**A. Eltwati:** Conceptualization, Data Curation, Formal analysis, Investigation, Methodology, Project administration, Resources, Software, Supervision, Validation, Visualization, Writing - Original Draft, Writing - Review & Editing – **M. Enieb:** Conceptualization, Data Curation, Formal analysis, Investigation, Methodology, Project administration, Resources, Software, Supervision, Validation, Visualization, Writing - Original Draft, Writing - Review & Editing – **S. Ahmeed:** Conceptualization, Data Curation, Software – **Z. Al-Saffar:** Conceptualization, Data Curation, Formal analysis, Methodology, Resources, Software, Validation, Visualization – **A. Mohamed:** Conceptualization, Data Curation, Formal analysis, Methodology, Resources, Software, Validation, Visualization

#### References

[1] Ziari, H., Orouei, M., Divandari, H., & Yousefi, A. (2021). Mechanical characterization of warm mix

- asphalt mixtures made with RAP and Para-fiber additive. *Construction and Building Materials*, 279, 122456. <https://doi.org/10.1016/j.conbuildmat.2021.122456>
- [2] Enieb, M., Al-Jumaili, M. A. H., Al-Jameel, H. A. E., & Eltwati, A. S. (2021, August). Sustainability of using reclaimed asphalt pavement: based-reviewed evidence. In *Journal of Physics: Conference Series*. 1973(1), 012242. <https://doi.org/10.1088/1742-6596/1973/1/012242>
- [3] Diab, A., Sangiorgi, C., Enieb, M., & You, Z. (2016). A conditioning method to evaluate moisture influence on the durability of asphalt mixture materials. *Canadian Journal of Civil Engineering*, 43(11), 943-948. <http://dx.doi.org/10.1139/cjce-2016-0153>
- [4] Al-Saffar, Z. H., Yaacob, H., Katman, H. Y., Mohd Satar, M. K. I., Bilema, M., Putra Jaya, R., Eltwati, A. S. & Radeef, H. R. (2021). A Review on the Durability of Recycled Asphalt Mixtures Embraced with Rejuvenators. *Sustainability*, 13(16), 8970. <https://doi.org/10.3390/su13168970>
- [5] Wróbel, M., Wozzuk, A., Ratajczak, M., & Franus, W. (2021). Properties of reclaimed asphalt pavement mixture with organic rejuvenator. *Construction and Building Materials*, 271, 121514. <https://doi.org/10.1016/j.conbuildmat.2020.121514>
- [6] Zhang, J., Guo, C., Chen, T., Zhang, W., Yao, K., Fan, C., Liang, M., Guo, C. & Yao, Z. (2021). Evaluation on the mechanical performance of recycled asphalt mixtures incorporated with high percentage of RAP and self-developed rejuvenators. *Construction and Building Materials*, 269, 121337. <https://doi.org/10.1016/j.conbuildmat.2020.121337>
- [7] Yousefi, A. A., Sobhi, S., Aliha, M. M., Pirmohammad, S., & Haghshenas, H. F. (2021). Cracking properties of warm mix asphalts containing reclaimed asphalt pavement and recycling agents under different loading modes. *Construction and Building Materials*, 300, 124130. <https://doi.org/10.1016/j.conbuildmat.2021.124130>
- [8] Burbano-Garcia, C., Hurtado, A., Silva, Y. F., Delvasto, S., & Araya-Letelier, G. (2021). Utilization of waste engine oil for expanded clay aggregate production and assessment of its influence on lightweight concrete properties. *Construction and Building Materials*, 273, 121677. <https://doi.org/10.1016/j.conbuildmat.2020.121677>
- [9] Bai, T., Hu, Z. A., Hu, X., Liu, Y., Fuentes, L., & Walubita, L. F. (2020). Rejuvenation of short-term aged asphalt-binder using waste engine oil. *Canadian Journal of Civil Engineering*, 47(7), 822-832. <http://dx.doi.org/10.1139/cjce-2019-0268>
- [10] Ren, S., Liu, X., Fan, W., Qian, C., Nan, G., & Erkens, S. (2021). Investigating the effects of waste oil and styrene-butadiene rubber on restoring and improving the viscoelastic, compatibility, and aging properties of aged asphalt. *Construction and Building Materials*, 269, 121338. <https://doi.org/10.1016/j.conbuildmat.2020.121338>
- [11] Devulapalli, L., Kothandaraman, S., & Sarang, G. (2022). Microstructural characterisation of reclaimed asphalt pavement with rejuvenators. *International Journal of Pavement Engineering*, 23(4), 1038-1049. <https://doi.org/10.1080/10298436.2020.1788027>
- [12] Majidifard, H., Tabatabaee, N., & Buttler, W. (2019). Investigating short-term and long-term binder performance of high-RAP mixtures containing waste cooking oil. *Journal of Traffic and Transportation Engineering (English Edition)*, 6(4), 396-406. <https://doi.org/10.1016/j.jtte.2018.11.002>
- [13] Mohi Ud Din, I., & Mir, M. S. (2021). Laboratory Study on the use of Reclaimed Asphalt Pavement and Copper Slag in Warm Mix Asphalt Pavements using Waste Engine Oil as a Rejuvenator. *International Journal of Pavement Research and Technology*, 1-13. <https://doi.org/10.1007/s42947-021-00036-y>
- [14] Wang, F., Fang, Y., Chen, Z., & Wei, H. (2018, June). Effect of waste engine oil on asphalt reclaimed properties. In *AIP conference proceedings*. 1973(1), 020012. <https://doi.org/10.1063/1.5041396>
- [15] Al-Saffar, Z. H., Yaacob, H., Satar, M. K. I. M., Kamarudin, S. N. N., Mahmud, M. Z. H., Ismail, C. R., Hassan, S. A. & Mashros, N. (2021). A review on the usage of waste engine oil with aged asphalt as a rejuvenating agent. *Materials Today: Proceedings*, 42, 2374-2380. <https://doi.org/10.1016/j.matpr.2020.12.330>
- [16] Tahami, S. A., Mirhosseini, A. F., Dessouky, S., Mork, H., & Kavussi, A. (2019). The use of high content of fine crumb rubber in asphalt mixes using dry process. *Construction and Building Materials*, 222, 643-653. <https://doi.org/10.1016/j.conbuildmat.2019.06.180>
- [17] Eltwati A.S., Hossein A., Nasr D. (2020). Effect of Crumb Rubber Particles on the Properties of Asphalt. *Lecture Notes in Civil Engineering*, 59, 43-52 [https://doi.org/10.1007/978-981-15-1193-6\\_5](https://doi.org/10.1007/978-981-15-1193-6_5)
- [18] Eltwati A.S., Saad I., Elsaiti A. (2019). The Effect of Crumb Rubber on Properties of Asphalt Mix by Dry Process. *The International Journal of Engineering and Information Technology (IJEIT)*, 5(1)
- [19] Fakhri, M., Amosoltani, E., & Aliha, M. R. M. (2017). Crack behavior analysis of roller compacted concrete mixtures containing reclaimed asphalt pavement and crumb rubber. *Engineering Fracture Mechanics*, 180, 43-59. <https://doi.org/10.1016/j.engfracmech.2017.05.011>

- [20] Yousefi, A., Behnood, A., Nowruz, A., & Haghshenas, H. (2021). Performance evaluation of asphalt mixtures containing warm mix asphalt (WMA) additives and reclaimed asphalt pavement (RAP). *Construction and Building Materials*, 268, 121200. <https://doi.org/10.1016/j.conbuildmat.2020.121200>
- [21] Duarte, G. M., & Faxina, A. L. (2021). Asphalt concrete mixtures modified with polymeric waste by the wet and dry processes: A literature review. *Construction and Building Materials*, 312, 125408. <https://doi.org/10.1016/j.conbuildmat.2021.125408>
- [22] Dong, R., Zhao, M., & Tang, N. (2019). Characterization of crumb tire rubber lightly pyrolyzed in waste cooking oil and the properties of its modified bitumen. *Construction and Building Materials*, 195, 10-18. <https://doi.org/10.1016/j.conbuildmat.2018.11.044>
- [23] Duarte, G. M., & Faxina, A. L. (2021). High-temperature rheological properties of asphalt binders modified with recycled low-density polyethylene and crumb rubber. *Construction and Building Materials*, 298, 123852. <https://doi.org/10.1016/j.conbuildmat.2021.123852>
- [24] Lin, P., Huang, W., Li, Y., Tang, N., & Xiao, F. (2017). Investigation of influence factors on low temperature properties of SBS modified asphalt. *Construction and Building Materials*, 154, 609-622. <http://dx.doi.org/10.1016/j.conbuildmat.2017.06.118>
- [25] Tauste, R., Moreno-Navarro, F., Sol-Sánchez, M., & Rubio-Gámez, M. C. (2018). Understanding the bitumen ageing phenomenon: A review. *Construction and Building Materials*, 192, 593-609. <https://doi.org/10.1016/j.conbuildmat.2018.10.169>
- [26] ASTM. (2020). *D5 / D5M-20, Standard Test Method for Penetration of Bituminous Materials*. ASTM International, West Conshohocken, PA.
- [27] ASTM. (2020). *D36 / D36M-14, Standard Test Method for Softening Point of Bitumen (Ring-and-Ball Apparatus)*. ASTM International, West Conshohocken, PA.
- [28] ASTM. (2017). *D113-17, Standard Test Method for Ductility of Asphalt Materials*. ASTM International, West Conshohocken, PA.
- [29] ASTM. (2021). *D70 / D70M-21, Standard Test Method for Specific Gravity and Density of Semi-Solid Asphalt Binder (Pycnometer Method)*. ASTM International, West Conshohocken, PA.
- [30] Jahanbakhsh, H., Karimi, M. M., Naseri, H., & Nejad, F. M. (2020). Sustainable asphalt concrete containing high reclaimed asphalt pavements and recycling agents: Performance assessment, cost analysis, and environmental impact. *Journal of Cleaner Production*, 244, 118837. <https://doi.org/10.1016/j.jclepro.2019.118837>
- [31] Hunter R.N., Self A., Read J. (2015). *The Shell Bitumen Handbook*.
- [32] Roberts F.L., Kandhal P.S., Brown E.R., Lee D.-Y., Kennedy T.W. (1991). Hot mix asphalt materials, mixture design and construction.
- [33] ASTM. D6931, *Standard Test Method for Indirect Tensile (IDT) Strength of Asphalt Mixtures*. American society for testing and materials 2017.
- [34] Lv, Q., Huang, W., Sadek, H., Xiao, F., & Yan, C. (2019). Investigation of the rutting performance of various modified asphalt mixtures using the Hamburg Wheel-Tracking Device test and Multiple Stress Creep Recovery test. *Construction and Building Materials*, 206, 62-70. <https://doi.org/10.1016/j.conbuildmat.2019.02.015>
- [35] Enieb, M., Eltwati, A., & Al-Jumaili, M. A. (2021). Temperature sensitivity and performance evaluation of asphalt cement incorporating different types of waste polymers. *Journal of Innovative Transportation*, 2(2). <https://doi.org/10.53635/jit.984159>
- [36] Moghadas Nejad, F., Azarhoosh, A., Hamed, G. H., & Roshani, H. (2014). Rutting performance prediction of warm mix asphalt containing reclaimed asphalt pavements. *Road Materials and Pavement Design*, 15(1), 207-219. <https://doi.org/10.1080/14680629.2013.868820>
- [37] Eltwati, A. S., Enieb, M., Al-Saffar, Z. H., & Mohamed, A. (2021). Effect of glass fibers and waste engine oil on the properties of RAP asphalt concretes. *International Journal of Pavement Engineering*, 1-12. <https://doi.org/10.1080/10298436.2021.2001815>
- [38] Eltwati, A. S., Enieb, M., Mohamed, A., Al-Saffar, Z. H., & Al-Jumaili, M. A. (2021, August). A laboratory study of the effect of fiberglass additive on the behavioural properties of RAP asphalt mixtures. In *Journal of Physics: Conference Series*. 1973(1), 012241. <https://doi.org/10.1088/1742-6596/1973/1/012241>
- [39] Enieb, M., Cengizhan, A., Karahancer, S., & Eltwati, A. (2022). Evaluation Of Physical-Rheological Properties of Nano Titanium Dioxide Modified Asphalt Binder and Rutting Resistance of Modified Mixture. *International Journal of Pavement Research and Technology*, 1-19. <https://doi.org/10.1007/s42947-021-00131-0>
- [40] Copeland A. (2011) Reclaimed asphalt pavement in asphalt mixtures: State of the practice. United States. Federal Highway Administration.
- [41] Im, S., Zhou, F., Lee, R., & Scullion, T. (2014). Impacts of rejuvenators on performance and engineering properties of asphalt mixtures containing recycled materials. *Construction and Building Materials*, 53, 596-603. <https://doi.org/10.1016/j.conbuildmat.2013.12.025>



## Progressive failure analysis of partially pre-stressed concrete railway sleepers

Ferhat Çeçen<sup>a</sup> , Bekir Aktaş<sup>b,\*</sup> 

<sup>a</sup> TCDD (Turkish State Railways), Concrete Sleeper Factory, Sivas, Turkey 

<sup>b</sup> Erciyes University, Civil Engineering Department, Kayseri, Turkey 

### Highlights

- 50% more compression stress occurs in the A-type sleepers compared to N-type
- $F_{rr}$  value in more detail concerning the concrete tensile strength
- 25% higher stresses occur in A-type design than N-type design under  $Fr_{0.05}$  load

### Abstract

Billions of sleepers are used on railways around the world today. As the importance of railways in the transportation sector is increasing, the demand for sleepers is also increasing. Although wooden and steel sleepers were used in rail systems in the past, today the most widely used sleeper type in the world is reinforced concrete sleepers. Among these reinforced concrete sleepers, pre-stressed sleepers are the most widely used, popular type of sleeper that can be produced in many countries. The two main production methods of pre-stressed sleepers are the ribbed reinforced system and the non-ribbed reinforced anchor plated system. In this study, B70 type pre-stressed concrete sleepers, have been investigated with the positive moment determination tests at the rail seat with progressive failure observations according to EN 13230-2:2016 standard. After tests, detailed cracking, failure, and fatigue analyzes under increasing test loads were performed with ANSYS® finite element analysis results for both types of pre-stressed sleepers. According to results, A-type sleepers have 50% more compression stress at the first crack formation load ( $F_{rr}$ ) than N-type sleepers and According to the first 0.05 mm permanent crack formation load ( $Fr_{0.05}$ ), it is seen that 25% higher stresses occur in A-type design than N-type design under  $Fr_{0.05}$  load. The results obtained through the analysis have been compared with the actual field measurement results, which have become more and more popular in the world in recent years. In this direction, various suggestions have been made for the development of concrete railway sleeper models.

### Information

Received:

05.05.2022

Received in revised:

09.06.2022

Accepted:

09.06.2022

**Keywords:** concrete sleeper, prestressed concrete, cracking mechanics, ANSYS

### 1. Introduction

The components of classical ballasted railways are categorized as superstructure and infrastructure. As shown in Figure 1, while the rails and the sleepers are "superstructure" components; the ballast and the formation layer are "infrastructure" components. Sleepers are of great importance in protecting the road geometry and transferring the loads and vibrations taken from the rails to the infrastructure by damping [1]. Although wooden and steel sleepers were used in rail systems in the past, today the most widely used sleeper type in the world is the reinforced concrete sleeper. Among the reinforced concrete sleepers, pre-stressed

reinforced concrete sleepers are the most widely used, popular type of sleeper that can be produced in many countries shown in Figure 1 [2].



Figure 1. Representation of conventional ballasted railway components

\*Corresponding author: [baktas@erciyes.edu.tr](mailto:baktas@erciyes.edu.tr) (B. Aktas), +90 352 207 6666

In Figure 2, the most widely used production methods of these pre-stressed reinforced concrete sleepers in the world are presented. With the long-line production process as shown in Figure 2.a, pre-stressed main-line sleepers and turnout bearers can be produced in the desired cross-section and length, including rectangular sections. Mold plates and accessories used in this process are easily available. As can be seen in Figure 2.a; High-capacity pre-stressing equipment is needed to keep the pre-stressing force strong along the tens of meters long production line. Produced concrete blocks, depending on the factory capacity, are cut in desired intermediate lengths. Therefore, it is practical to produce turnout bearer sets containing different lengths of sleepers. In this process, HTS (high tensile strength) class pre-stressing strands (tendons) are used, which can be obtained easily and at a low cost in the market. In addition to the ease of supply, these strands are self-ribbed and do not require a special process, anchoring equipment, or labor for their use, providing significant advantages in sleeper production cost.

The carousel process is given in Figure 2.b requires high automation. In this process, a cyclic process is carried out in the form of "cleaning of sleeper molds-assembly of connection materials-pre-processing-concrete placement - rotating disassembly-cleaning of sleeper molds". In this system, steel molds are usually used that serve to produce 2 or 4 sleepers together and are strong enough to meet the pre-stress force. In this way, 2-4 sleepers in each cycle are prepared for the curing process. In this process, the used molds bear the pre-tensioning force until the concrete is cured, so sleeper molds are needed for about 14 hours production process. Unlike the long line process, the HTS rods in this process must be subjected to special workmanship such as screw-cutting, bending, mounting the anchor plates, etc. depending on sleeper sizes and production process. With the carousel system, the pre-stressed sleepers can be produced with pre-tensioned or post-tensioned processes. But the carousel system is not feasible for turnout bearers since the connection material positions and sleeper lengths of the turnout bearers vary greatly. According to the results of the tests performed on the sleepers with various reinforcement and anchorage structures given in Figure 3; It is stated that the ultimate strength of sleepers in fatigue tests is higher with the use of anchored and/or a larger number of reinforcements usage [3]. Pre-stressed sleepers can be produced differently from these systems and even with various reinforcement numbers or anchorage processes. More reinforcement number usage has a bigger bonding surface, also ribbed surface produces smaller or no anchor plate usage. A bigger anchor surface produces smaller early concrete strength and longer fatigue life.



Figure 2. Common production methods of pre-stressed reinforced concrete sleepers: a. Pre-stressed sleeper production with long-line system b. Pre-stressed sleeper production with a carousel system



Figure 3. Various reinforcement and anchorage mechanisms in carousel sleeper production system a. Without ribbed-with anchor plate, b. Ribbed-with anchor plate, c. Ribbed-without anchor plate [3]

In pre-stressed sleepers, the reason for applying the pre-stress is to prevent or limit bending cracks in service [4]. As it is known, tensile stresses occur in structural elements under simple bending. Since the tensile strength of concrete materials is low to be neglected, steel-reinforced concrete structures have been developed. In reinforced concrete elements, the concrete material needs to be deformed to meet the tensile stresses by engaging the reinforcements, and cracks are inevitable when the deformation level in the concrete increases. In pre-stressed designs, before the service loads affect the structural element, pre-stressing compression is provided to the element over the reinforcements. This pre-compression capacity eliminates the tensile stresses "partially" or "completely" [1]. The phrases "partially" and "completely" in this definition make great differences in terms of product performance. Early pre-stressed concrete designers focused on eliminating tensile stresses in structural members. This design method is called a "fully pre-stressed" system. However, loads above the calculated design load may occur in the elements that cannot be fully predicted (such as railway sleepers). Also, it is quite complicated to predict whether tensile stress occurs in the concrete section, depending on the distribution variability of the minimum and maximum moment occurring along the cross-section. Therefore, either complex and expensive sections are used or the pre-stressing force is increased to stay in the safe zone [5]. As the experience of pre-stressed systems increases, it has been seen that the elements to be designed between the classical non-pre-stressed system and the fully pre-stressed system offer many advantages. These systems, where tensile stresses in concrete are allowed at a specified level under full-service load, are called "partially pre-stressed" designs. With this method, a more economical design can be applied with smaller cross-sectional areas and less reinforcement can be used. Also,

under ultimate load, partially pre-stressed systems show higher ductility than fully pre-stressed systems and can absorb more energy against high dynamic loads such as earthquakes or explosions [6].

Today, the partially pre-stressing design philosophy explained above is applied in pre-stressed railway sleepers. In the pre-stressed railway sleepers, as long as the train does not affect the road, there is a pre-stressing compression continuously acting towards the sleeper center. Thanks to this additional capacity, no cracks occur in the sleeper (invisible because tensile stresses occur, but it does not exceed the crack resistance) up to the fatigue design load ( $F_{r0}$ ). While the train is affecting the road, this compression decreases repeatedly towards zero and if the impact load is more than the pre-stressing capacity (decompression load), it starts to increase as a negative (tensile stress) [1]. Despite the advantages mentioned above, partially pre-stressed members reaching their fatigue limit under repetitive reversible loads can be a cause for concern. Cracks are formed in the partially pre-stressed elements under the effect of the first dynamic loads, and in the following dynamic loads, cracks with a lower value than the first appear again. Although it is predicted that in fully pre-stressed uncracked sections, the pre-stressing force (due to the stretching of the concrete, relaxation of the reinforcement, etc.) will decrease by approximately 14%, this value is quite high in the cracked sections [6]. For these reasons, sleepers produced with the partially pre-stressing process are not desired to be exposed to loads higher than the fatigue design load ( $F_{r0}$ ), and according to standards such as EN 13230-1 / 2 on railway sleepers, loads above this limit are called exceptional ( $F_{r0.05}$ ), so that a very small number of them allowed in the service life [7]. Because under these repetitive reversible loads, early fatigue and higher capacity losses are seen [1].

In the literature, there are many studies on the comparison of the impact loads on the railway with the pre-stressing capacity of the sleepers, and also on the insufficiency of the capacity of the existing sleepers, a sample study is presented in Figure 4 [8]. When trainloads affect the partially pre-stressed railway sleepers, the pre-stressing capacity is reached first (decompression), then the first cracks become visible after a little more load is carried due to the cracking resistance of the concrete section ( $F_{rr}$ ). As can be seen from Figure 4, before the cracking load of the partially pre-stressed sleepers starts, the pre-stressing capacity is used up and the "decompression" load is exceeded. After this load value, firstly elastic and then plastic deformations are observed in concrete and reinforcement. Also, as can be seen from Figure 4, the record of the loads exceeding the pre-stressing capacity is quite higher than the allowed capacity of standards, and even in the short period of 12 months, the number of loads exceeding the cracking load reaches tens of thousands. Like this study, various field measurement studies have been carried out on railways

in recent years and the adequacy of the sleeper design loads calculated with empirical approaches in the past has been questioned. Indeed, it will not be fully correct to compare field record peak values with the static and fatigue test results of existing sleepers. Because the characteristics of the real railway conditions such as strain rate, load duration, and support conditions are greatly different from the tests in question. On the other hand, depending on the railway operating capacity, the number of load repetitions is also quite high, and there are different effects in different parts of the sections and continuous changes in the forced sections. So, the service life is highly predicted to decrease under these high magnitude impact loads. Meanwhile, the real cracking mechanics of the railway sleepers need to be examined in more detail with special analysis methods that include the real load characteristics of railways.

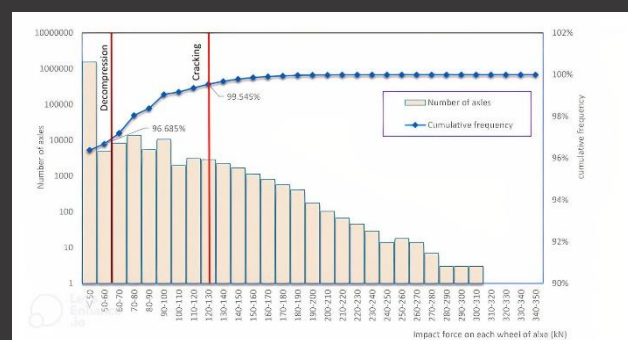


Figure 4. The cumulative frequency of the load values that create decompression and crack initiation in sleepers according to railway field measurement records [8]

The applied partially pre-stressing compression to the sleepers and the use of corrosive steel reinforcements bring many disadvantages, even in the most modern designs. For this reason, cracks that progress gradually (and completely or partially closed with the effect of pre-stressing force after the train passes) cannot be prevented in the sleepers. With the effect of these cracks, the concrete is damaged and the pre-stress force decreases, and the chlorine ions penetrating the concrete cause corrosion in the pre-stressing steel. Therefore, sleeper life ends before the planned (40/50-year) service life [9]. While corrosion can occur even when there is no crack in reinforced concrete structures, it becomes easier to occur with the formation of cracks. And it's well known that a material's corrosion susceptibility changes significantly after being pre-stressed or bent, and cyclic loading of a material accelerates stress-induced corrosion cracking. Also, the diameter of the used reinforcement for pre-stressing is smaller than the conventional system. For this reason, a small amount of local corrosion or a thin layer of corrosion causes a significant decrease in the reinforcement cross-sectional area and consequently, it breaks [6]. There are various studies in the literature on corrosion damages occurring in pre-stressed railway sleepers [10].

In this study, B70 type pre-stressed concrete railway sleepers, have been investigated with the positive moment determination tests at the rail seat with progressive failure observations according to EN 13230-2:2016 standard. After tests, detailed cracking, failure, and fatigue analyzes under increasing test loads were performed with ANSYS® finite element analysis results for both types of pre-stressed sleepers. The results obtained through the analysis have been compared with the actual field measurement results, which have become more and more popular in the world in recent years. In this direction, various suggestions have been made for the development of the concrete railway sleeper models.

## 2. Material and Method

### 2.1. B70 type railway sleepers and positive moment determination test procedure

The descriptive codes of the reinforced concrete sleepers developed and expanded in Germany contain a number after the letter B. The letter B stands for concrete and the number after the letter represents the design year of the sleeper [11]. The curing process of manufactured B70 type sleepers and fresh concrete samples was carried out following EN 13230-1:2016. After the curing period of 28 days, the sleepers were subjected to the "static positive moment determination tests at the rail seat", which is given the test setup and loading procedure in Figure 5 per EN 13230-2:2016. In this standard, the conditions of static loading positive moment determination test on the rail seat to be applied in the acceptance and design of pre-stressed sleepers are given [7]. In the test phase, the support distance is 60 cm. Loading is carried out until the first crack is detected ( $F_{rr}$ ) or up to the load value determined by the railway establishment ( $F_{r0}$ ). Then, the load is increased by 10 kN and kept constant for 10 seconds to 5 minutes, then the load is removed and the crack is checked with a lens. In this way, when the load is removed with 10 kN increments, if a plastic crack above a thickness of 0.05 mm is detected, the second recording data ( $F_{r0.05}$ ) of the experiment is found. Finally, by continuing the loading-unloading procedure, the breaking load ( $F_{rB}$ ) is recorded, where the section cannot carry more load [12].

### 2.2. Finite element modelling for cracking mechanics analysis

ANSYS® 2020 R1 software, which is widely used worldwide, was used in the finite element analysis conducted within the scope of this study. In sleeper modeling, only half of the whole body affected by the test supports was modeled using the "symmetry" feature in the ANSYS Mechanical module, and thus analyzes was easily performed. In concrete material modeling, "Concrete NL" material from the "non-linear engineering materials" in the material library and the Drucker-Prager model from the "GeoMechanical" material models in the

toolbox menu were used. In finite element analysis, 3 methods are widely used in modeling the reinforcement. These are the assumption of smeared reinforcement based on the reinforcement cross-section ratio, the embedded reinforcement assumption, where the reinforcement is assumed as axle elements combined with concrete, and the discrete reinforcement assumptions made up of completely separate elements. In this study, apart from these three models, separate modeling, which provides a more detailed analysis, was applied as shown in Figure 6. Thanks to this model, is better than the discrete reinforcement assumption, which is shown as the most effective of the common reinforcement models; Instead of one-dimensional "truss" elements, three-dimensional "solid" elements were used and all the loads that the reinforcement would be subjected to were taken into account. As can be seen in Figure 6, in the finite element analysis, two different production methods with ribbed-reinforced and plane reinforced-anchor plated sleeper types are modeled and detailed stress and deformation characteristics are analyzed mutually. The issue of mesh overlap, which is of great importance in reinforcement modeling in a ribbed design, is provided with the shared topology option in the SpaceClaim® software that comes with the ANSYS program. For the anchor-plated model, frictionless contact modeling was applied without sharing the topology between the reinforcements and concrete, and full adherence was applied by modeling "bonded contact" only on the reinforcement-anchor plates-concrete contact surfaces.

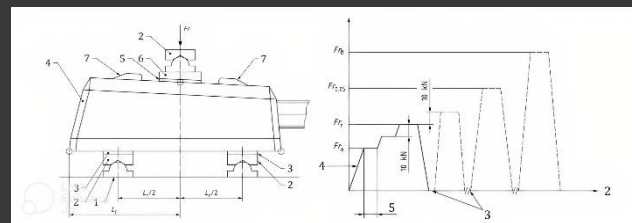


Figure 5. Test setup (left) and static test procedure (right) (left figure; 1: rigid support, 2: articulated support, 3: resilient pad, 4: sleeper, 5: standard rail pad, 6: tapered packing, 7: lateral stop and base plate (figure on the right; 1: load, 2: time, 3: crack control, 4: loading speed limit 120 kN / min, 5: standby time (10 seconds-5 minutes)) [7]

To create stress-strain curves for HTS class steel reinforcement, the yield strength values of 1585 MPa and tangent modulus 2628 MPa were entered in the "bi-linear" material properties section of the Structural Steel NL material in the ANSYS material library. In the modeling of the pre-stressing force, the "inistate" command of ANSYS software was used. Before the test load is affected, a separate "load-step" is created and pre-deformation is given in the direction of the reinforcement axis. In the tested B70 type sleepers, 4 pieces of HTS class steel reinforcement with a diameter of 9.4 mm were used. Approximately 75.53 Newton pre-stress force is applied to these rods, and approximately 1090 MPa pre-stress compression is provided in each reinforcement. ANSYS

Solid 186 and Solid 187 element types were preferred for modeling both concrete elements and reinforcements. These high-quality elements have 3 dimensional, 20 points, and quadratic deformation capability and are recommended for detailed analysis. These 20 separate points have freedom in 3 axes and offer advantages of plasticity, hyper elasticity, creep, large deflections, pre-stressed design, and layered composite modeling [13]. To fully obtain the advantages specified from Solid 186-187 elements and to avoid convergence problems, a "hex-dominant" (hexagonal) mesh configuration was applied as suggested in the literature and shown in Figure 6 [14]. Finite element mesh sizes have a significant effect on higher or lower stress results. The use of a smaller mesh size reduces the energy distribution, so it can show the breaking load less than it is, however, the use of a bigger mesh size can show the breaking load higher than it is because it reduces the crack development [15]. After the mesh operation is done, the evaluation criteria should be accessed under the "mesh metric" line in the "statistics" section. At this stage, the "skewness criterion" is the most widely used and valid. A skewness value up to 0.94 can be accepted, but if it is above this, a poor-quality mesh can be mentioned [16]. In analyzes, the mesh quality was calculated by ANSYS as 0.686 for the ribbed design and as 0.234 for the un-ribbed design in terms of "skewness", and analyzes were continued, seeing that they are of sufficient quality. The higher mesh quality of the un-ribbed design is due to the lack of reinforcement-concrete topology sharing.

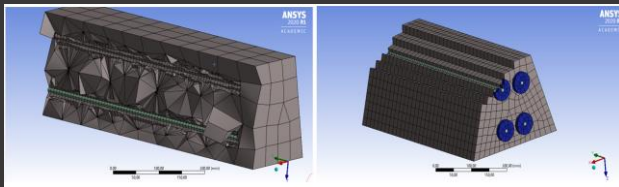


Figure 6. Finite element mesh modeling of two different pre-stressed sleeper types; ribbed-reinforced type (left) and plane reinforced-anchor plated type (right)

It is of great importance to define the support conditions correctly during the sleeper tests to obtain an accurate and unique solution. In EN 13230-2 tests, the bearings have a rectangular contact surface that can rotate in the bending direction, with a width of 10 cm, and also plastic interfaces are used to reduce local crushes [7]. In this context, simulation analyzes were carried out for various support conditions. It was observed that the more accurate support condition, which gives the same results as the applied experiments, is "remote displacement" supports of 10 cm width that allow horizontal (UY) movement and rotation in the X-axis on both supports. Also, it was decided to apply a "remote force" condition in which only vertical (UZ) movement is allowed on the rail support with the hydraulic press loading assembly and "deformable" interfaces instead of "rigid" intermediate elements in all three interfaces. As given in Figure 7; In both remote displacement and remote force applications, contact surfaces are modeled not in the "line" form,

which is frequently encountered in practice, but real area (surface) definitions of 10 cm width are made and more realistic results are obtained. To obtain detailed results with non-linear modeling during analyzes, the "large deflections" setting was turned on in the analysis settings. Also, to prevent convergence error, the applied load is increased not in one step, but in 20 stages (load steps), and these stages are divided for the second time with a minimum of 3 "sub steps". In this way, the stiffness matrix in each stage is updated before moving to the next load stage [17]. During analyzes, the non-linear Full Newton-Raphson iteration procedure and automatic time stepping were set, allowing the stiffness matrix to be updated at each iteration. After all these adjustments, the solution time of the software has increased considerably. However, in this way, ANSYS software was able to predict and control the new loading steps based on the past solution records and advance the load steps per the accuracy of the convergence graph.

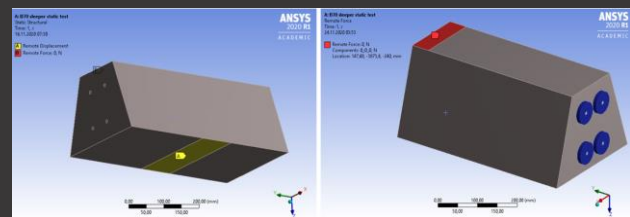


Figure 7. Modeling of support and loading conditions of static test setup in accordance with EN 13230-2.

### 3. Findings

#### 3.1. Experimental test results

During the sleeper production, 150x150x150 mm cube and 150x300 mm cylinder samples were taken from the pre-stressed reinforced concrete sleepers, and compression and splitting tensile tests were performed. Test results and used other parameters in ANSYS finite element analyzes are presented in Table 1. The compressive strength result of concrete was determined 68.0 MPa which is C50 / 60 class in accordance with the TS EN 206-1 standard [18]. So, in finite element analyzes, the 50 MPa value was entered as characteristic compressive strength. According to the test results given in Table 1 and TS 500: February 2000 equation 3.2, the elasticity module of the concrete was calculated as 36981 MPa [19]. The characteristic splitting tensile strength of concrete was calculated as 4.16 MPa in accordance with TS EN 206-1 standard from the splitting tensile test results with an average value of 4.66 MPa and the direct (uniaxial) tensile strength is calculated as 2.77 MPa by dividing this value by 1.5 [19]. The Poisson's ratio is equal to a constant value as long as the strains remain within elastic limits. This value is approximately 0.15 - 0.20 for concrete [20]. In the literature, there are studies on the use of a 0.25 value for beam elements under bending [17]. The Poisson's ratio of concrete has an important effect on the correct calculation of the reinforcement stresses, and

in this study, the average value of 0.25 was used considering the bending load of the sleepers during the tests and the lower trapezoidal sleeper section dimensions. Obtained load value-crack thickness measurements with lens and crack width gauge after each loading step are presented in Table 2 and sample test visuals are presented in Figure 8-Figure 12. The crack development mechanism in the figures is shown in blue for cracks that are closed after the load is removed, and in red if a permanent crack of 0.05 mm or more remains after the load is removed. As can be seen; the first crack observation (Frr) in sleepers occurred in the 190-210 kN range. After the loads at this level are removed, the cracks close again with the effect of the pre-stressing compression. The first crack formation load value is important in proving the adequacy of the pre-stressing compression in pre-stressed sleepers, and it is routinely checked with random samples taken from the daily production of factories. The next part of the test is referred to as "design approval tests" and does not require routine control without process changes [7]. The second design parameter requested in EN 13230-2 is the load value at which a 0.05 mm permanent (plastic) crack occurs (Fr0.05), and the last parameter is the breaking load (FrB), as can be seen in Figure 5 [7].

Table 1. Cube and cylinder concrete test results and finite element model parameters

Concrete parameters	Results
Compressive strength test result (average)	68,0 MPa
Concrete compressive strength class (EN 206-1)	C50/60
Concrete characteristic compressive strength (fck)	50 MPa
Initial elasticity modulus of concrete (TS 500)	36981 MPa
Poisson's ratio of concrete (from literature [17])	0,25
Splitting tensile strength test result (average)	4,66 MPa
Characteristic tensile strength (EN 206-1)	2,77

Table 2. EN 13230-2 Static loading positive moment determination test results at rail seat

Test / measurement parameters	Results (kN)
First crack formation (Frr)	205
First crack onset after 230 kN load	190
First crack onset after 240 kN load	160
First crack onset after 250 kN load	150
First crack onset after 260 kN load	130
First crack onset after 270 kN load	130
First crack onset after 350 kN load	70
First crack onset after 360 kN load	70
Permanent crack of 0.05 mm (Fr0,05)	288
Permanent crack of 0.20 mm	300
Permanent crack of 0.35 mm	330
Permanent crack of 0.50 mm (Fr0,5)	350



Figure 8. First crack formation (Frr = 190 kN) and permanent crack load (Fr0.05=300 kN) after the test load is removed



Figure 9. Cracks occurred at the first crack formation load (Fr = 210 kN) and permanent crack load (Fr0.05=290 kN) after the test load is removed

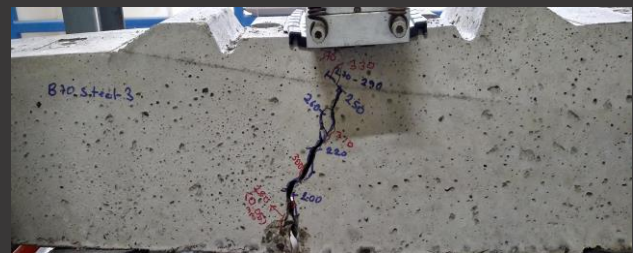


Figure 10. Cracks occurring under 380 kN static load, while the test load continues to act

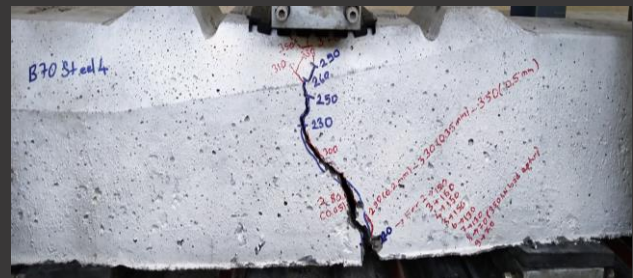


Figure 11. Permanent crack levels occurred under the effect of various test stages and the change in the first crack formation load under the effect of increasing loads

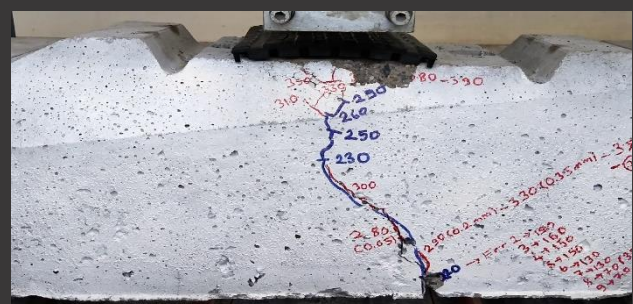


Figure 12. Cracks in the sleeper after 430 kN breaking load (FrB)

### 3.2. Finite element analysis results

Analyzes were performed on two major types of B70 sleepers. The first one is the sleeper containing ribbed reinforcements without an anchor plate and will be referred to as "N-type". The second type is an anchorage plated sleeper containing un-ribbed reinforcements and will be referred to as "A-type".

3.2.1. Stresses in concrete and reinforcement under the effect of pre-stressing force

The equivalent stress distribution in the concrete and reinforcements for the N-type sleeper under the effect of the pre-stressing force is shown in Figure 13. As is seen in this figure, approximately 1135 MPa equivalent tensile stress occurs in the reinforcement due to the pre-stressing force. This value coincides with the previously calculated 1090 MPa pre-stress strength for physical applications. Local stress concentrations are largely minimized since the topology is shared during the geometry arrangement. In finite element analyzes that require more detail, it is possible to completely prevent stress concentrations by making local mesh settings (refinement, etc.) of the mesh sizes at the contact locations of concrete and reinforcement. As is seen in Figure 13, after the pre-stressing process, while the compression stresses exceed 40 MPa near the concrete-reinforcement contact surface, this value decreases to approximately 7.2 MPa in the upper compression lobe and shows the minimum value at the bottom face because of the B70 type sleepers' trapezoidal cross-section. As can be seen from Figure 15, where the equivalent stress distribution for this location is given, there is only 5.7 MPa compressive stress at this location.

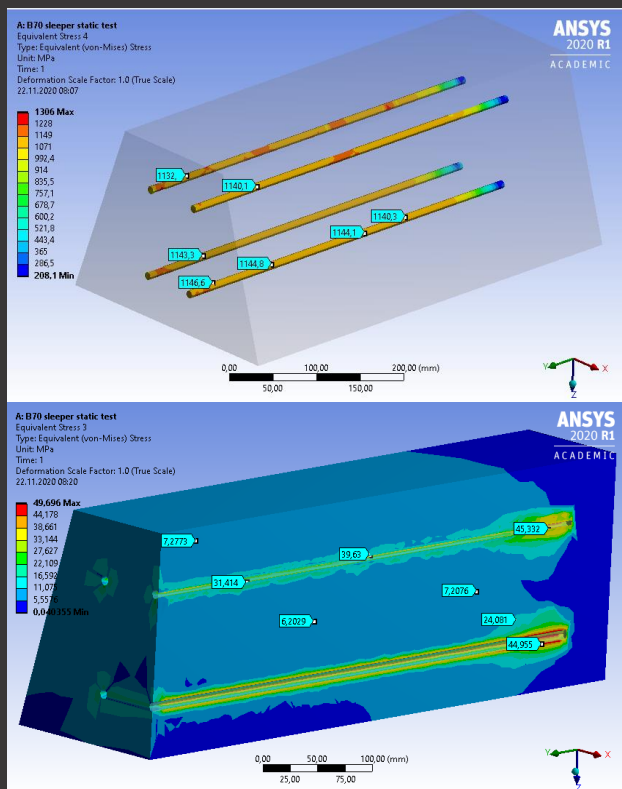


Figure 13. N-type sleeper equivalent stress (MPa) distributions of concrete and reinforcements after pre-stressing

The equivalent stress distribution in the concrete and reinforcements for the A-type sleeper under the effect of the pre-stressing force is shown in Figure 14. As is seen in this figure, approximately 1127 MPa equivalent tensile stress occurs in the reinforcement due to the pre-

stressing force. This value coincides with the previously calculated 1090 MPa pre-stress strength for physical applications. As can be seen in Figure 14, the stresses seem higher than normal at some contact points where the reinforcement transfers load to the anchor plates. As stated before, in detailed finite element analyzes, it is possible to prevent stress concentrations with local mesh settings at contact locations. As is seen in Figure 14, after the pre-stressing process, while the compression stresses exceed 40 MPa near the anchor plate contact surface, this value decreases to approximately 7.5 MPa in the upper compression lobe and shows the minimum value at the bottom face because of the B70 type sleepers' trapezoidal cross-section. As can be seen from Figure 15, where the equivalent stress distribution for this location is given, there is only 5.2 MPa compressive stress at this location. Considering the yield strength (1350-1600 MPa) and fatigue limit (1200-1400 MPa) of the used HTS type reinforcements, for both N and A-type sleepers, the pre-stressing force is limited up to 75 kN (1100 MPa) for each of 4 reinforcements each with a cross-section of 69 mm<sup>2</sup>. So, a total of approximately 320 kN pre-stressing force is obtained. However, a smaller number of reinforcement strands/rods or smaller anchor plates can cause higher stresses than the 20-35 MPa fatigue limit of sleeper concrete. The total circumference (reinforcement-concrete contact surface) of the 4 pieces of 9.4 mm diameter reinforcement in the analyzed sleepers is 118 mm. If the number of pieces is increased without decreasing the total reinforcement cross-section in sleeper production, for example, if 12 pieces of reinforcement with a diameter of 5.4 mm are used, the total circumference increases above 200 mm. In this case, the contact stresses that will occur in the concrete will decrease considerably, and the need for early high strength during production will also decrease. A similar approach is valid for the anchor plate geometry.

3.2.2. Determination of decompression load

After modeling the pre-stressing force, static loading positive moment test analysis at the sleeper rail seat was started. As the load acting at the rail seat increases, the pre-stress compression effects of the reinforcements gradually decrease and change direction at a certain point (decompression load value) theoretically beginning to work like typical non-stressed reinforced concrete structures. However, this is valid for the places near cracked areas, and different behaviors occur in different locations of the sleepers. The stress sensor is modeled at the bottom of the mid-span cross-section of the sleeper to determine the load value (decompression), where the pre-stressing force is finished and the reinforcements start to carry loads like non-pre-stressed designs and the resulting stress distributions are presented in Figure 15. As can be seen from this figure, the "compression" stress occurring in the concrete section under the effect of the pre-stressing gradually decreases with the effect of the test load acting on the sleeper rail seat. It starts to

increase as "tensile" stress, reaching the bottom point at a load value of about 82 kN in N-type and 76 kN in A-type.

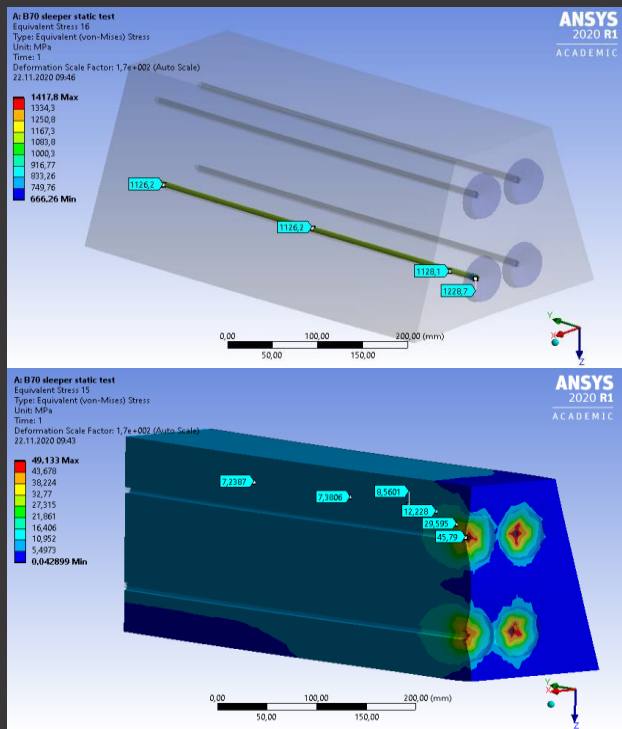


Figure 14. A-type sleeper equivalent stress (MPa) distributions of concrete and reinforcements after prestressing

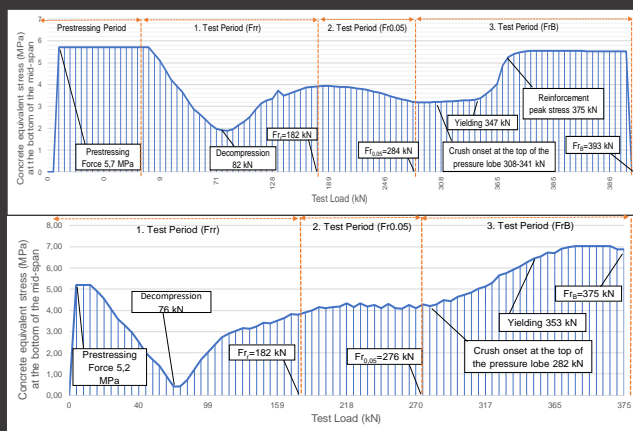


Figure 15. Concrete equivalent stress (MPa) at the bottom of the mid-span cross-section of the sleeper vs test load (kN) curves; up-side: N-type sleeper, down-side: A-type sleeper

The fatigue life of pre-stressed sleepers at loads under decompression capacity is considered to be "infinite" if a correct reinforcement and anchoring mechanism is applied. According to the recent field records given as an example in Figure 4, 96.685% of the loads affecting the sleepers are under the decompression capacity. In other words, it can be said that the sleepers will be subjected to an average of 300 million load repetitions during the targeted service life of 50 years, 290 million of them are within pre-stressing capacity.

### 3.2.3. Determination of first crack formation loads ( $F_r$ )

Experiments to detect cracks in pre-stressed sleepers can often be misleading. The reason for this is that the cracks remain at the micro level due to the effect of the pre-stressing compression. Therefore, in EN 13230-2, test loading speed is limited to 120 kN / min during the first crack detection and inspection with a lens that can magnify at least 20 times is required instead of naked-eye inspection [7]. Another point to be considered is, as specified in EN 13230-1; In the first crack formation detection, only the cracks "reaching a height of 15 mm from the sleeper bottom" should be recorded [7]. The first crack ( $F_r$ ) observed in the laboratory tests was determined as 205 kN. In the finite element model, as can be seen from Figure 15, where the equivalent stress (MPa) distribution of the concrete material at the bottom of the mid-span cross-section of the sleeper is given, the first crack formation loads are determined as 182 kN in both the sleeper types. The reason why the early deformations are higher in N-type sleepers is that the reinforcement contact surfaces to which the pre-stressing force is transferred in N-type sleepers are much closer to the midsole point where the deformation sensor is located than the anchorage plates in A-type sleepers. The detected first crack formation loads were also confirmed and compared with Figure 16 where the maximum principal and equivalent stress distributions of concrete and reinforcements are given. In the maximum principal stress distributions locations that exceed the tensile strength of concrete of 2.77 MPa are shown with red fill. The determined values by finite element analyzes are slightly lower than the laboratory test results. This difference may have resulted from the sensitive crack formation process as stated above and the use of safety coefficients or with various assumptions in finite element analyzes. As can be seen from Figure 16, at the first crack formation load, 50% more compression stress occurs in the upper lobe of A-type sleepers compared to N-type sleepers. When the stress values of the reinforcement are examined, it is seen that there is approximately 10% more stress in the A-type sleepers, also the maximum value occurred near the anchor plates, unlike the "N-type". It can be also seen from the maximum principal stress distributions in Figure 16 that in N-type sleepers there are fewer cracks and less width. The service life of pre-stressed sleepers at loads above the decompression capacity begins to decrease due to fatigue. As before-mentioned, above the decompression capacity, the stresses in the pre-stressing reinforcement change direction (transforming). Today, fatigue tests with 3-5 Hz frequency and approximately 50-150 kN load cycles are performed in sleeper design approval tests. For example, according to EN 13230 standard, after 2 million loading cycles, a maximum loss of 45 kN in breaking load is anticipated for B70 type sleepers (from 375 kN to 330 kN). In case of operating conditions above the number and magnitude stipulated in the standard, this loss of capacity will increase even more. According to the recent field

records given as an example in Figure 4, 3.315% of the loads affecting the sleepers are above the decompression capacity. In other words, it can be said that the sleepers will be subjected to an average of 300 million load repetitions during the targeted service life of 50 years, and approximately 10 million of them are expected to remain above the decompression value. While high magnitude railway loads have a very high strain rate and their duration of action is quite short, depending on the railway operating capacity, the number of load repetitions is also quite high, and on the other hand, as can be seen from Figure 16, there are different effects in different parts of the sections and continuous changes in the forced sections. So, the service life begins to decrease due to fatigue.

In line with the analysis results presented so far, it can be easily inferred that the first crack capacity ( $F_{r1}$ ) consists of the combination of the pre-stressing capacity (decompression) and the tensile strength of the concrete. As given in Table 2, it has been determined by laboratory tests that the load value observed in the first crack formation load decreases from 206 kN to 130 kN after a few load repetitions within the elastic deformation limits of the reinforcement (210-277 kN). In the experiments conducted with non-pre-stressed sleepers produced with equivalent concrete and cross-section of B70 type pre-stressed sleepers, it was observed that the first crack formation could occur at a load of approximately 120 kN [1]. The combination of an average cracking strength of concrete of 120 kN and a decompression load of 76-82 kN coincides with the average first crack formation load of 206 kN obtained in laboratory tests. Concrete technology in the years when B70 and similar type sleepers were designed, has developed considerably today. Therefore, a revision of the first crack formation load test is required considering the tensile strength of today's high-performance concrete. As determined, the visible crack starting load value ( $F_{r1}$ ) in pre-stressed sleepers is the combination of pre-stressing capacity (decompression) and tensile strength of concrete. Today, the minimum value ( $F_{r0}$ ) of the first crack formation load that can be observed in B70 type pre-stressed reinforced concrete sleepers has been determined as 150 kN [12]. The cracking strength of concrete depends on many factors such as maximum aggregate diameter, granulometry, aggregate surface roughness, and placement quality and can give results in a wide range (50-150 kN). If concrete with a cracking resistance of 75 kN and above is used, it may not be fully controlled in routine controls whether the pre-stressing force is applied sufficiently or not. In other words, the first crack starting a load of 150 kN capacity or a big part of it can easily be reached in sleepers with high tensile strength of concrete, although not enough pre-stressing force is applied. In this respect, it is thought that it would be more appropriate to control the first crack formation load ( $F_{rr}$ ) value in more detail with the concrete tensile strength used in sleeper production.

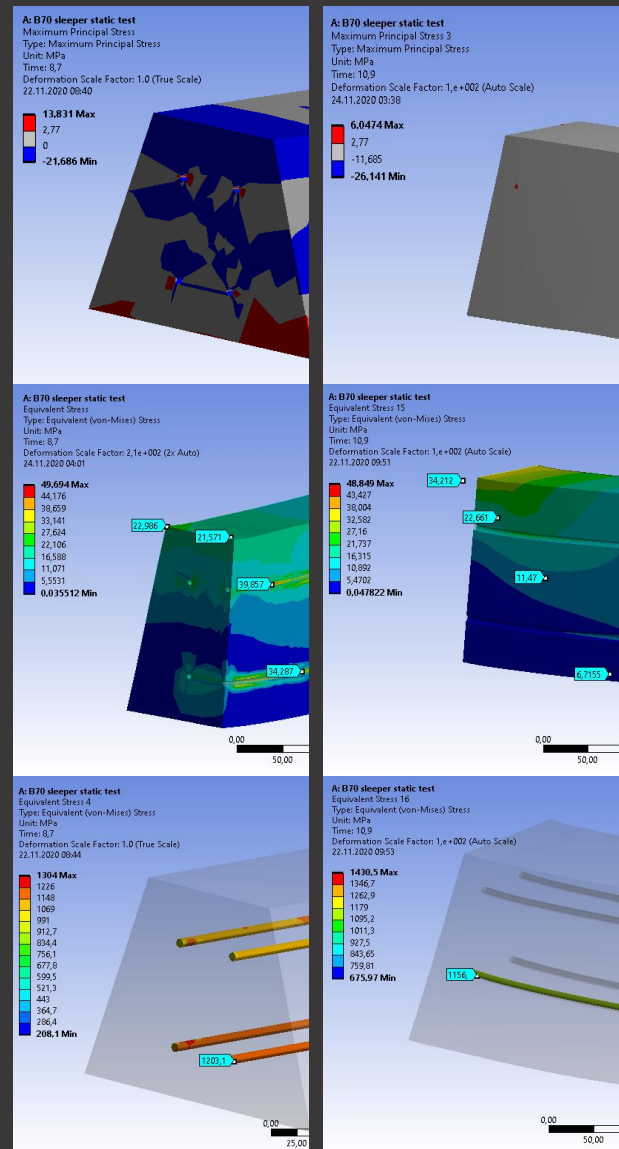


Figure 16. Comparative analysis results of concrete and reinforcements at  $F_{r1}$  test loads in N-type sleeper (left-sides) and A-type sleeper (right-sides)

### 3.2.4. Determination of permanent crack loads ( $F_{r0.05}$ )

Another parameter required in TS EN 13230-2 is the permanent crack ( $F_{r0.05}$ ) load of 0.05 mm thickness. Since cracks occurring up to this load value occur within elastic limits, it closes again with the effect of pre-stressing pressure after removing the load. According to laboratory tests, elastic cracks extend to the middle of the sleeper height at approximately 200-250 kN and the upper part of the compression lobe around 270-300 kN. At the same time (270-300 kN), cracks with a thickness of 0.05 mm ( $F_{r0.05}$ ) that do not fully close (plastic) when the load is removed are started to be detected at the bottom of the mid-span. In finite element analysis, the permanent crack formation loads are detected and compared with Figure 17 where the maximum principal and equivalent stress distributions of concrete and reinforcements are given. In the maximum principal stress distributions locations that exceed the tensile strength of concrete of 2.77 MPa are shown with red fill. Accordingly, the  $F_{r0.05}$  load was

determined as 282 kN in the N-type design and 276 kN in the A-type design. Obtained values significantly coincide with the physical test result of 288 kN. According to results, similar to the first crack formation load, the number, and width of the cracks are lesser but thicker at un-ribbed A-type design, as can be seen from maximum principal stress distributions. As regards concrete stresses, it is seen that 25% higher stresses occur in the A-type design than in the N-type design under the  $F_{r0.05}$  load. In the A-type design, it is seen that the ultimate strength of 50 MPa has begun to be exceeded both in the compression lobe and near the anchor plate. The occurrence of higher deformations has a great effect on the occurrence of this situation in the A-type design. In terms of reinforcement stresses, the stresses at the mid-span cross-section of the N-type sleepers and the stresses at the anchor plate location in the A-type sleepers gave similar results. As seen, the level of deformation occurring in A-type sleepers is much higher than in type N.

According to the results of the field measurements given in Figure 4, 99.545% of the loads to be placed on the sleepers are below the first crack formation load value. In other words, it can be estimated that the sleepers will be exposed to approximately 1.3 million loads above the first crack formation load value during the targeted 50-year service life. As can be seen from Figure 17, at the  $F_{r0.05}$  load level, stresses exceeding the fatigue limit occur in the reinforcement (1400-1500 MPa) and concrete (40-50 MPa) in both types of pre-stressed sleeper. An important point, while high magnitude railway loads have a very high strain rate and their duration of action is quite short, depending on the railway operating capacity, the number of load repetitions is also quite high, and also as can be seen from Figure 17, there are different effects in different parts of the sections and continuous changes in the forced sections. So, the service life begins to rapidly decrease due to fatigue, corrosion, and loss of pre-stress force. Under these repetitive reversible loads, early fatigue and higher capacity losses are seen [1]. As a result of laboratory experiments as can be seen in Figure 12, it was determined that the load value of first crack formation ( $F_r$ ) starting in pre-stressed sleepers decreased up to 70 kN. Considering that sleepers are exposed to millions of load repetitions on railways, these capacity losses, determined by a few load repetitions, can be expected to occur at a higher level in actual field use. It is also stated in the FIB-CEB categorization; that it is recommended to apply "full pre-stressing" in structures that will be exposed to fatigue due to dynamic load or corrosive effects [5]. On the other hand, in the sleeper modeling in this study, it was assumed that the existing pre-stressing force did not decrease. However, the pre-stressing force already decreases in the long term due to factors such as relaxation, creep, and thermal expansion, so in real conditions, pre-stressed sleepers' fatigue life is more affected.

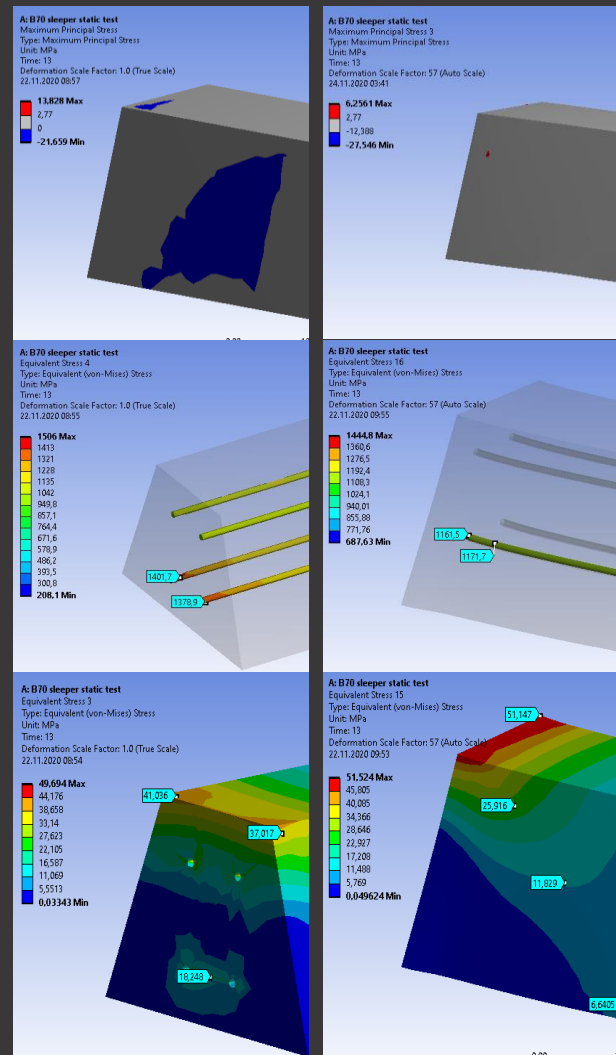


Figure 17. Comparative analysis results of concrete and reinforcements at  $F_{r0.05}$  test loads in N-type sleeper (left-sides) and A-type sleeper (right-sides)

### 3.2.5. Determination of breaking loads ( $F_B$ ) and development suggestions

The last parameter required in TS EN 13230-2 is the peak load ( $F_B$ ) that the sleeper cannot carry more. Equivalent stress distributions of concrete and reinforcements at this load level are given in Figure 18. For the N-type sleepers, the yielding at reinforcement contact surfaces is reached at 347 kN and the ultimate strength is reached at 375 kN load levels. At a load of 393 kN, the deformations increase so that finite element analysis cannot continue. Afterward, the analysis is terminated automatically by the software since convergence cannot be made. Since the desired information in the standard was reached (peak load value that cannot carry more load), the current analysis was found to be sufficient. In A-type sleepers, reinforcement yield starts at the level of 353 kN test load and rupture does not occur in the reinforcements until the end of the analysis. So, it has been determined that the breaking load of A-type sleepers is 393 kN and can show high deformations. As a matter of fact, in physical tests, the breaking condition of A-type sleepers is reached by crushing the concrete compression lobe. The breaking

loads can be also seen in Figure 15, where concrete equivalent stress development at the bottom of the mid-span cross-section is given. These values are slightly lower than the average breaking load of 430 kN obtained in physical tests. This difference may have resulted from the use of safety coefficients or various assumptions in finite element analyzes. As a result, according to both laboratory experiments and ANSYS finite element analyzes, it was observed that the  $F_{r0.05}$  permanent crack formation load increased significantly as the reinforcement cross-section area increased [1]. At the same time, it is stated that the ultimate strength of sleepers in fatigue tests is higher by using anchored and/or more individual reinforcement [3], and it is shown with the fatigue tests performed on conventional and partially pre-stressed elements with equal final moment capacity, it was observed that the fatigue strength of the partially pre-stressed elements was lower [6]. Therefore, it is considered that reinforcement number and cross-section areas and anchorage geometries, including the non-pre-stressed sleeper production alternative, should be designed taking into account the actual field measurements and reinforcement fatigue limits.

standard. After tests, detailed cracking, failure, and fatigue analyzes under increasing test loads were performed with ANSYS® finite element analysis results for both types of pre-stressed sleepers. The results obtained through the analysis have been compared with the actual field measurement results, which have become more and more popular in the world in recent years. The findings obtained from the experiments and finite element analyzes are given below;

It was observed that the finite element model and the laboratory test results overlapped substantially. Local stress concentrations can be largely minimized with the ANSYS® SpaceClaim® topology sharing option. On the other hand, pre-stressed concrete sleeper failure stages; The decompression load; The first elastic crack formation load ( $F_r$ ); The first 0.05 mm permanent crack formation load ( $F_{r0.05}$ ); and the breaking load ( $F_B$ ) values can be accurately predicted with ANSYS® finite element analysis.

In recent years, various field measurement studies have been carried out on railways and the adequacy of the sleeper design loads calculated with empirical approaches in the past has been questioned. Studies in this direction have been encouraged in the postmodern EN 13230-6: 2020 standard. In this study, the results of a recent field measurement were used for sample analysis. Each railway organization should measure the stress, strain, and acceleration data to analyze its road parameters and maintenance status. More realistic results will be obtained as the location variation and measurement time are increased in the measurements to be made.

When the sample field measurement results are examined, it is first seen that impact loads several times higher than the decompression and cracking capacities of pre-stressed concrete railway sleepers occur frequently. But it will not be fully correct to compare field record peak values with the static and fatigue test results of existing sleepers. Because the characteristics of the real railway conditions such as strain rate, load duration, and support conditions are greatly different from the tests in question. However, depending on the railway operating capacity, the number of load repetitions is also quite high, and on the other hand, there are different effects in different parts of the sections and continuous changes in the forced sections. So, the service life begins to decrease due to fatigue.

The fatigue life of pre-stressed sleepers at loads under decompression capacity (for B70 type ~75 kN) is considered to be “infinite” if a correct reinforcement and anchoring mechanism is applied. According to recent field records, over 96% of the loads affecting the sleepers are under decompression capacity.

For the loads above the decompression and below the minimum first crack formation loads (75-150 kN) service life of pre-stressed sleepers begins to decrease due to

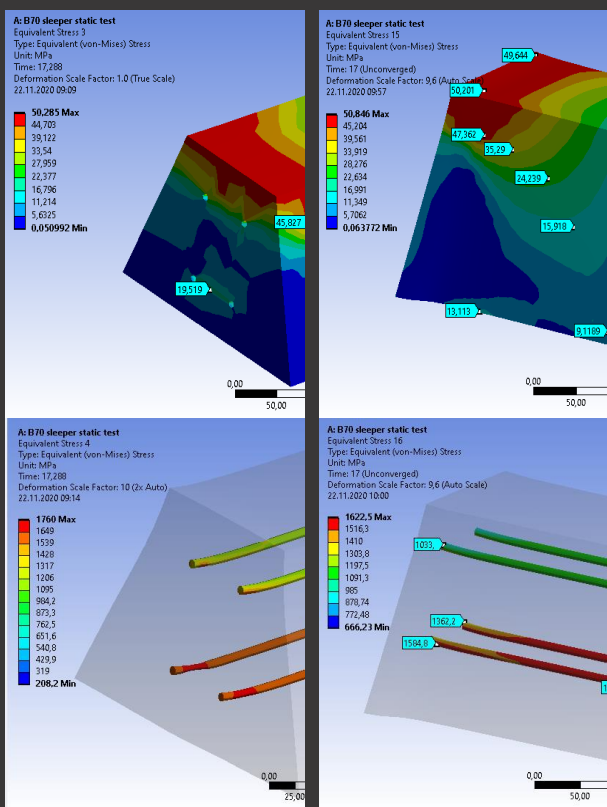


Figure 18. Comparative analysis results of concrete and reinforcements at  $F_{rB}$  test loads in N-type sleeper (left-sides) and A-type sleeper (right-sides)

#### 4. Conclusion and Discussion

In this study, B70 type pre-stressed concrete sleepers, have been investigated with the positive moment determination tests at the rail seat with progressive failure observations according to EN 13230-2:2016

fatigue. According to recent field records, 3.315% of the loads (approximately 10 million) affecting the sleepers are above the decompression capacity. In this region, the stresses in the pre-stressing reinforcement change direction (transforming), and repetitive reversible loads cause early fatigue. According to EN 13230 standard, after 2 million loading cycles, a maximum loss of 45 kN in breaking load is anticipated for B70 type sleepers (from 375 kN to 330 kN).

Loads above the first elastic crack formation load and below the first 0.05 mm plastic crack formation load (150-270 kN), decrease the service life of pre-stressed sleepers relatively faster. According to recent field records, 0.455% of the loads (approximately 1.3 million) affecting the sleepers are above the first elastic cracking load value. It has been determined by laboratory tests that the load value observed in the first crack formation load decreases from 206 kN to 130 kN after a few load repetitions within this region. According to EN 13230 standard, after approximately sixty thousand loads, a maximum loss of 45 kN in breaking load is anticipated for B70 type sleepers (from 375 kN to 330 kN).

Loads above the first 0.05 mm plastic crack formation load and below the breaking load (270-375 kN), decrease the service life of pre-stressed sleepers quite faster. It has been determined by laboratory tests that the load value observed in the first crack formation load decreases from 206 kN to 70 kN after a few load repetitions within this region. According to the recent field records, approximately one thousand loads affecting the sleepers are above the first 0.05 mm plastic cracking load value. According to standards such as EN 13230-1 / 2 on railway sleepers, loads in this region are called exceptional, so a very small number of them are allowed in the service life. With the effect of these cracks, the concrete is damaged, the pre-stress force decreases, and the chlorine ions penetrating the concrete cause corrosion in the pre-stressing steel. Therefore, sleeper life ends before the planned (40/50-year) service life.

A revision of the first crack formation load test is required considering the tensile strength of today's high-performance concrete. Concrete technology in the years when B70 and similar type sleepers were designed, has developed considerably today. The first crack starting load required by the standards or a big part of it can easily be reached in sleepers with high tensile strength of concrete, although not enough pre-stressing force is applied. In this respect, it is thought that it would be more appropriate to control the first crack formation load ( $F_{r1}$ ) value in more detail with the concrete tensile strength used in sleeper production.

According to the first crack formation load ( $F_{r1}$ ), 50% more compression stress occurs in the A-type sleepers compared to N-type sleepers. And at the first 0.05 mm permanent crack formation load ( $F_{r0.05}$ ), it is seen that

25% higher stresses occur in A-type design than N-type design under  $F_{r0.05}$  load. It is also seen that at this load level in the A-type design, the ultimate strength of 50 MPa has begun to be exceeded both in the compression lobe and near the anchor plate. On the other hand, the number, and width of the cracks are lesser but thicker in an un-ribbed A-type design. Therefore, the ribbed reinforced sleeper design appears to be more advantageous than the non-ribbed anchor plated design in many respects.

In fatigue tests performed on conventional (non-pre-stressed) and partially pre-stressed elements with equal final moment capacity, it was observed that the fatigue strength of the partially pre-stressed elements was lower. Therefore, it is considered that reinforcement number and cross-section areas and anchorage geometries, including the non-pre-stressed sleeper production alternative, should be designed taking into account the actual field measurements and reinforcement fatigue limits.

As a result, the prepared model provides many advantages in matters such as investigating what kind of stress and deformations occur in the background of concrete and reinforcements during the beginning of elastic and plastic cracks in the sleeper and reaching the final strength.

#### Acknowledgments

We would like to thank Turkish State Railways (TCDD) for their support and cooperation.

#### Declaration of Interest Statement

**F. Çeçen:** Conceptualization, Data curation, Formal analysis, Funding acquisition, Investigation, Methodology, Project administration, Resources, Software, Supervision, Validation, Visualization, Writing – original draft, Writing – review & editing – **B. Aktaş:** Conceptualization, Data curation, Formal analysis, Funding acquisition, Investigation, Methodology, Project administration, Resources, Software, Supervision, Validation, Visualization, Writing – original draft, Writing – review & editing – B.

#### Author Contribution Statement

The authors declare that they have no known competing financial interests or personal relationships that could have appeared to influence the work reported in this paper.

## References

- [1] Çeçen F. & Aktaş B. (2021). New Generation Railway Sleepers and Experimental Research of Domestic FRP Reinforcement Use (in Turkish). *Railway Engineering* (13), 53-64. <https://doi.org/10.47072/demiryolu.803452>
- [2] Taherinezhad, J., Sofi, M., Mendis, P., & Ngo, T. (2017). Strain rates in prestressed concrete sleepers and effects on cracking loads. *Electronic Journal of Structural Engineering*, 17, 65-75. <https://ejsei.com/EJSE/article/view/220>
- [3] Derkowski, W., Słyś, B., & Szmit, M. (2014). Effect Of Strands'anchorage System In PC Railway Sleepers On Behaviour Of Its Rail Seat Zone–Experimental Research.. *8th International Conference of AMCM*, 16-18 June, Wrocław, Poland, 101-108. <https://www.infona.pl/resource/bwmeta1.element.baztech-86d049c1-10f0-4aa2-bd38-9ad624eb5722>
- [4] Özcan A. İ., Özden B., Ölçer B. & Gamlı F. D. (2018). Betonarme Traverslerin Gelişimi. *Demiryolu Mühendisliği Dergisi*, 18 (2), 40-44. Available: <https://dergipark.org.tr/tr/pub/demiryolu/issue/35609/448512>
- [5] Thürlimann B. (1968). Partially Pre-stressed Members. *International Association for Bridge and Structural Engineering (IABSE) Congress*, 9-14 September, New York, 474-487. <http://doi.org/10.5169/seals-8717>
- [6] The American Concrete Institute-ASCE Committee 423, State-Of-The-Art Report on Partially Pre-stressed Concrete: *ACI* 423.5R-99. [http://civilwares.free.fr/ACI/MCP04/4235r\\_99.pdf](http://civilwares.free.fr/ACI/MCP04/4235r_99.pdf)
- [7] Anonymous, EN 13230-1/2 Standard. 2016. Railway applications, Track, Concrete sleepers and bearers, General requirements/ Pre-stressed Monoblock sleepers. European Committee for Standardization (CEN)
- [8] You, R., & Kaewunruen, S. (2019). Evaluation of remaining fatigue life of concrete sleeper based on field loading conditions. *Engineering Failure Analysis*, 105, 70-86. <https://doi.org/10.1016/j.engfailanal.2019.06.086>
- [9] Çeçen F. (2019). New railway concrete sleeper research about using carbon fiber reinforced polymer rebars with non-pre-stressed and mono-block process, (in Turkish). Master Thesis. Gaziosmanpaşa University. 156s, Tokat. <https://www.researchgate.net/publication/344163677>
- [10] Jokūbaitis, A., Marčiukaitis, G., & Valivonis, J. (2016). Influence of technological and environmental factors on the behaviour of the reinforcement anchorage zone of prestressed concrete sleepers. *Construction and building materials*, 121, 507-518. <http://dx.doi.org/10.1016/j.conbuildmat.2016.06.025>
- [11] Bezgin N. Ö., (2016). Stresses developed by the vertical forces acting on ballasted railway tracks. *16. Geotechnical Engineering Congress*. 13-14 October. Erzurum, 1-10.
- [12] Çelik M. S. (2015). A Multifaced Analysis of Railway Sleepers and Scrutinize of Different Railway Sleepers on An Example Line (In Turkish). Master Thesis. *Istanbul Technical University*. 103s, İstanbul.
- [13] Budapest University of Technology and Economics, Department of Applied Mechanics, Index of /~gyebro/files/ans\_help\_v182. Accessed: 30.10.2020. [Online]. [https://www.mm.bme.hu/~gyebro/files/ans\\_help\\_v182/ans\\_elem/Hlp\\_E\\_SOLID186.html](https://www.mm.bme.hu/~gyebro/files/ans_help_v182/ans_elem/Hlp_E_SOLID186.html)
- [14] Wolanski A. J. (2004). Flexural behavior of reinforced and pre-stressed concrete beams using finite element analysis. *Marquette University*, Master of Science Thesis, Milwaukee, Wisconsin.
- [15] Shayanfar, M. A., Kheyroddin, A., & Mirza, M. S. (1997). Element size effects in nonlinear analysis of reinforced concrete members. *Computers & structures*, 62(2), 339-352. [https://doi.org/10.1016/S0045-7949\(96\)00007-7](https://doi.org/10.1016/S0045-7949(96)00007-7)
- [16] Ovalı İ. (2018). Ansys Workbench. 3. Edition. İstanbul. ISBN 978-605-9118-89-7.
- [17] Hammad, M. R. (2015). Non-linear Finite Element Analysis of Reinforced Concrete Beams Strengthened with Carbon Fiber-Reinforced Polymer (CFRP) Technique. *The Islamic University of Gaza*, Civil Engineering Department, Master of Science Thesis, 98s, 2015.
- [18] Anonymous, 2002. EN 206-1: Concrete- Part 1: Specification, performance, production and conformity. European Committee for Standardization (CEN)
- [19] Anonymous, 2000. TS 500: Requirements for design and construction of reinforced concrete structures. (in Turkish). Turkish Standards Institution, Ankara.
- [20] Dalgıç K. D. (2010). Axial Compressive Behaviour And Finite Element Analysis of Low Strength Concrete Confined by Low Modulus Glass Fibre Polymer (in Turkish), Master Thesis. *Istanbul Technical University*. 81s, İstanbul.
- [21] Giannakos, K. (2008). Damage of railway sleepers under dynamic loads: a case history from the Greek railway network. *Missouri University of Science and Technology*, Virginia, 1-11, <http://scholarsmine.mst.edu/icchge/6icchge/session08c/5>